PAXIP1 is regulated by NRF1 and is a prognosis-related biomarker in hepatocellular carcinoma

QIAN CHENG[1*], XIAO HAN[2*], HAO XIE[3*], YAN-LIN LIAO[4], FEI WANG[5], XIAO-YING CUI[6], CHAO JIANG[7] and CHENG-WAN ZHANG[2]

[1]Department of Pathogen Biology, Microbiology Division, Key Laboratory of Pathogen of Jiangsu Province Nanjing Medical University, Nanjing, Jiangsu 211166, P.R. China; [2]Department of Central Laboratory, The Affiliated Huaian No. 1 People's Hospital of Nanjing Medical University, Huai'an, Jiangsu 223300, P.R. China; [3]School of Life Science and Technology, Southeast University, Nanjing, Jiangsu 210018, P.R. China; [4]MEDx (Suzhou) Translation Medicine Co., Ltd., Suzhou, Jiangsu 215000, P.R. China; [5]Wuxi Mental Health Center/Wuxi Central Rehabilitation Hospital, Wuxi School of Medicine, Jiangnan University, Wuxi, Jiangsu 214122, P.R. China; [6]Affiliated Hospital of Integrated Traditional Chinese and Western Medicine, Nanjing University of Chinese Medicine, Nanjing, Jiangsu 210029, P.R. China; [7]Department of Oncology, The Affiliated Huaian No. 1 People's Hospital of Nanjing Medical University, Huai'an, Jiangsu 223300, P.R. China

Received June 21, 2024; Accepted November 13, 2024

DOI: 10.3892/br.2024.1916

Abstract. Hepatocellular carcinoma (HCC) is characterized by a poor prognosis globally. PAX-interacting protein 1 (PAXIP1) serves a key role in the development of numerous human cancer types. Nevertheless, its specific involvement in HCC remains poorly understood. Public repository systems (Integrative Molecular Database of HCC, Gene Expression Omnibus, The Cancer Genome Atlas, University of Alabama at Birmingham Cancer Data Analysis Portal, Tumor Immune Estimation Resource and Human Protein Atlas) were utilized to explore PAXIP1 expression in HCC and evaluate the prognostic value of PAXIP1 in patients with HCC. PAXIP1 expression was investigated, and a notable relationship between PAXIP1 expression and various cancer types was found through analysis of The Cancer Genome Atlas data. More specifically, patients with HCC and lower PAXIP1 levels had improved survival rates. Furthermore, using LinkedOmics, the co-expression network of PAXIP1 in HCC was determined. Colocalization analysis of PAXIP1 using chromatin immunoprecipitation-sequencing data suggested that PAXIP1 might act as a cofactor for MYB proto-oncogene like 2 or FOXO1 in HCC. In addition, by predicting and analyzing the potential transcription factors related to PAXIP1, nuclear respiratory factor 1 was identified as a factor upstream of PAXIP1 in HCC. Notably, PAXIP1 expression exhibited a positive association with the infiltration of $CD4^+$ and $CD8^+$ T cells, macrophages, neutrophils and myeloid dendritic cells. Furthermore, PAXIP1 expression was associated with a range of immune markers such as programmed cell death protein 1, programmed death-ligand 1 and cytotoxic T-lymphocyte associated protein 4 in HCC. The findings of the present study highlighted the prognostic relevance of PAXIP1 and its function in modulating immune cell recruitment in HCC.

Introduction

Hepatocellular carcinoma (HCC) is the predominant form of primary liver cancer, as well as the third leading cause of cancer-associated deaths worldwide (1,2). The prognosis of advanced HCC is particularly concerning because of high rates of recurrence and metastasis, which result in a poor 5-year survival rate worldwide (3). There are still gaps in the understanding of the molecular mechanisms that trigger HCC and facilitate its development, posing challenges for effective treatment (4). Consequently, a comprehensive understanding of these underlying mechanisms is crucial for advancing therapeutic strategies and improving patient outcomes.

PAX-interacting protein 1 (PAXIP1) was initially identified due to its interaction with paired box 2 (5) and other transcription factors (TFs) (6). Previous studies have highlighted the involvement of PAXIP1 in the DNA damage response and the regulation of histone modifications (7-10). Specifically, during the repair of double-stranded DNA breaks, PAXIP1, in conjunction with p53-binding protein 1 (53BP1), enhances non-homologous end-joining repair processes (10). Furthermore, PAXIP1 is crucial for the assembly of the histone methyltransferase complex at a Pax DNA-binding site, which is a significant aspect of mammalian development (6,9). PAXIP1 also interacts with the histone methyltransferase complex, suggesting that it serves a role in histone methylation and demethylation (7,9,11,12).

Correspondence to: Professor Cheng-Wan Zhang, Department of Central Laboratory, The Affiliated Huaian No. 1 People's Hospital of Nanjing Medical University, 1 Huanghe Road, Huai'an, Jiangsu 223300, P.R. China
E-mail: hayyzhchw@njmu.edu.cn

*Contributed equally

Key words: hepatocellular carcinoma, PAX-interacting protein 1, prognosis, immune cell infiltration

As a tandem BRCA1 C-terminal domain protein (5,13), PAXIP1 is associated with multiple types of cancer. For instance, PAXIP1 has been shown to function as a prognostic biomarker in ovarian cancer (14,15). Additionally, reduced PAXIP1 levels have been observed in patients diagnosed with breast cancer and an unfavorable prognosis (16). PAXIP1 has been demonstrated to modulate the cell response in lung cancer (17). Our previous study also demonstrated that PAXIP1 inhibited cell invasion via modulation of EPH receptor A2 (EphA2) expression in esophageal squamous cell carcinoma (18). Despite these findings, the expression patterns and precise role of PAXIP1 in HCC remain inadequately explored. Therefore, the protein and mRNA expression levels, prognostic significance and potential functions of PAXIP1 in HCC were assessed. Using multidimensional analysis and various public databases, an in-depth examination of the genomic alterations and functional networks pertaining to the role of PAXIP1 in HCC was conducted, thereby elucidating its involvement in tumor immunity.

Materials and methods

Cell culture and small interfering RNA (siRNA) transfection. The HuH-7 and PLC-PRF-5 human liver cancer cell lines were obtained from FuHeng Biology. HuH-7 cells were cultured in DMEM (cat. no. C11995500BT; Gibco; Thermo Fisher Scientific, Inc.) and PLC-PRF-5 cells were cultured in Minimum Essential Medium (MEM; cat. no. C11095500BT; Gibco; Thermo Fisher Scientific, Inc.). Cell media were supplemented with 10% FBS (cat. no. FBS500-S; Ausgenex Pty, Ltd.) and 1% penicillin/streptomycin (cat. no. 15140122; Gibco; Thermo Fisher Scientific, Inc.). Cells were kept at 37˚C in a humidity-controlled incubator with 5% CO_2 supplementation. All cell lines underwent rigorous verification for mycoplasma contamination and were confirmed to be free of contamination. The cells were authenticated using short tandem repeat analysis.

siRNA transfection was conducted using Lipofectam ine™ 2000 transfection reagent (cat. no. 52887; Invitrogen; Thermo Fisher Scientific, Inc.). All siRNA transfections were performed for 48 h at room temperature. HuH-7 and PLC-PRF-5 cells were cultured in 6-well plates to allow for adhesion and proliferation overnight. Before the introduction of the transfection agent, 1 ml serum-free DMEM/MEM was used to replace the medium. The scrambled control, CCCTC binding factor (CTCF) and nuclear respiratory factor 1 (NRF1) siRNA molecules were chemically synthesized by Nanjing GenScript Biotech Co., Ltd. For 6-well plates, 10 μl siRNA (20 μM) was dissolved in 5 μl siRNA transfection reagent and incubated for 5 min at room temperature. The aforementioned mixture was then introduced to the cells. After 12 h, 1 ml DMEM/MEM supplemented with 10% FBS was added to each well. Cells were seeded at a density of $6x10^5$ cells/well in 6-well culture plates. After 24 h, the cells were transfected with the siRNA for 48 h and then RNA was extracted. The siRNA sequences used were as follows: NRF1, 5'-GGAAACUUCGAGCCACGUU-3'; CTCF, 5'-GCGAAAGCAGCAUUCCUAUAU-3'; and control, 5'-UUCUCCGAACGUGUCACGU-3'.

Reverse transcription-quantitative PCR (RT-qPCR). Total RNA was extracted from HCC cells using RNeasy Kits (cat. no. 74104; Qiagen GmbH) according to the manufacturer's instructions. cDNA synthesis was conducted with the Primescript RT-reagent kit (cat. no. RR047A; Takara Bio, Inc.). The temperature and duration of reverse transcription were: 37˚C for 15 min and 85˚C for 5 sec. qPCR was performed using SYBR Premix Ex Taq (Takara Biotechnology Co., Ltd.) on an ABI7500 system (Applied Biosystems; Thermo Fisher Scientific, Inc.). The $2^{-\Delta\Delta Cq}$ method was utilized for data analysis, using β-actin for normalization (19,20). The thermocycling conditions were as follows: 95˚C for 5 min; 40 cycles of 95˚C for 15 sec and 60˚C for 30 sec; 1 cycle of 95˚C for 15 sec, 60˚C for 60 sec and 95˚C for 15 sec. The primer sequences used for qPCR were as follows: NRF1 forward, 5'-CCGGAAGAGGCAACAAACAC-3' and reverse, 5'-CTTGCTGTCCCACACGAGTAGT-3'; CTCF forward, 5'-CATCCAGCATCAGAAGTCACACA-3' and reverse, 5'-GCCTCTCCTGTCTACAAGCGTAA-3'; PAXIP1 forward, 5'-CCAGCTGTACGGACACTGAGG-3' and reverse, 5'-TTGTATGTCCCTGCTGGCTGT-3'; and β-actin forward, 5'-CACTCTTCCAGCCTTCCTTC-3' and reverse, 5'-GTACAGGTCTTTGCGGATGT-3'.

Chromatin immunoprecipitation-sequencing (ChIP-seq) analysis. ChIP-seq data for PAXIP1, MYB proto-oncogene like 2 (MYBL2) and FOXO1 were retrieved from the ChIP-Atlas database (http://chip-atlas.org/). The cutoff of broad peak call was $q<1x10^{-5}$ (transcription start site ±1 kb). These datasets (GSE32465 and GSE104247) (21,22) underwent further analysis using the ChIP-seq pipeline, mainly using the open-source BEDTools and deepTools software suites. BEDTools (version 2.29.2) (23) was employed for the genome arithmetic. The computeMatrix program within deepTools (version 3.4.3) (24) facilitated the calculation of scores across genome regions and generated intermediate files for subsequent visualization with plotHeatmap in deepTools. For genome annotation, R (version 4.1.0; http://www.r-project.org/) was used to analyze ChIPseeker (25). Gene Ontology (GO) analysis was implemented using Database for Annotation, Visualization and Integrated Discovery (DAVID) functional annotation tools (https://david.ncifcrf.gov/) (26). Metascape (https://metascape.org/) (27) was also employed to perform DisGeNET and PaGenBase enrichment analyses for PAXIP1 target genes.

Integrative molecular database of HCC (HCCDB) analysis. HCCDB (http://lifeome.net/database/hccdb/) is a comprehensive HCC expression atlas encompassing 15 publicly available HCC gene expression datasets, which collectively include 3,917 samples (28). This repository integrates data from prominent sources such as Gene Expression Omnibus, The Cancer Genome Atlas (TCGA) Liver HCC Project (TCGA-LIHC) and Liver Cancer-RIKEN, Japan Project from the International Cancer Genome Consortium. The HCCDB provides a platform for visualizing outcomes of various computational analyses, including differential expression analysis, as well as tissue- and tumor-specific expression assessments. The 15 HCC datasets were searched with the keyword 'PAXIP1'.

Cancer cell line encyclopedia, human protein atlas (HPA) and cBioPortal database analysis. The mRNA and protein expression profiles were downloaded from the Cancer Cell

Line Encyclopedia (https://depmap.org/portal/interactive/) and the HPA (https://www.proteinatlas.org/) (29,30). cBioPortal (https://www.cbioportal.org/), an open-source cancer genomics data platform, was used to analyze the mutations, copy-number alterations and gene expression of PAXIP1 in patients with HCC (31,32). Liver studies were selected and the keyword 'PAXIP1' was searched on the query page of the cBioPortal website (33-42).

LinkedOmics database analysis. Analysis of PAXIP1 expression in TCGA LIHC cohort was performed using the LinkedOmics database (http://www.linkedomics.org/) (43). Statistical analysis of PAXIP1 co-expression was conducted using Pearson's correlation coefficient, with results visualized using volcano plots, heatmaps and scatter plots. The functional module of the platform facilitates the examination of GO biological processes, Kyoto Encyclopedia of Genes and Genomes (KEGG) pathways, kinase-target enrichment, microRNA (miRNA)-target enrichment and TF-target enrichment via gene set enrichment analysis (GSEA).

Kaplan-Meier (KM) survival and nomogram analysis. KM survival analysis and plotting were performed using the R packages survival and survminer (https://CRAN.R-project.org/package=survminer). Analysis was performed using default parameters. The area under the curve (AUC) was analyzed using the R package timeROC (https://CRAN.R-project.org/package=timeROC). Based on prognostic clinical indicators and the survival analysis of the Cox regression model, age and pT_stage were entered into the risk model. The points against each factor were counted, and 1-, 3- and 5-year survival rates were also calculated. The nomogram was constructed using the rms package (https://CRAN.R-project.org/package=rms) (44). Additionally, the risk score was calculated as follows: Risk score=0.278 x PAXIP1 + 0.1718 x MYBL2 + 0.0175 x NRF1-0.2226 x FOXO1. Based on the risk score, patients with HCC were divided into the low-risk group and the high-risk group using the median risk score as the cutoff (45).

Prediction of TFs of PAXIP1. The human TF (hTF) target database (http://bioinfo.life.hust.edu.cn/hTFtarget#!/) represents an extensive resource dedicated to the regulation of hTFs and their respective targets (46). In the present study, this database was used to predict potential upstream TFs of PAXIP1. These TFs were then ranked according to their R- and P-value, providing a systematic evaluation of their potential regulatory roles. Find Individual Motif Occurrences (v4.10.0; https://meme-suite.org/meme/tools/fimo) was used to scan both the test and control sets, and then the numbers of recurrent motifs within the two sets were used to evaluate the significance of motifs for the TF (t-test with Bonferroni correction P<0.01) (46).

Tumor immune estimation resource (TIMER) database. The TIMER database (https://cistrome.shinyapps.io/timer/) was used to analyze the expression profile of PAXIP1 and immune cell presence in HCC. For gene expression levels, $\log_2$ transformed transcripts per million values were used.

Analysis of cancer data using the University of alabama at birmingham cancer data analysis portal (UALCAN) database and gene expression profiling interactive analysis (GEPIA). UALCAN (http://ualcan.path.uab.edu) uses level 3 RNA-sequencing and clinical data from TCGA data of HCC. This platform facilitates a comprehensive analysis of gene expression, comparing tumor samples with healthy control tissues and examining variations across diverse tumor subgroups classified by cancer stage, tumor grade or other clinicopathological parameters. UALCAN was used to examine mRNA expression levels according to the online instructions. GEPIA (http://gepia.cancer-pku.cn/) was used to investigate MYBL2 and FOXO1 expression in LIHC.

Visualization. Integrative Genomics Viewer (v2.17.0; http://software.broadinstitute.org/software/igv/home) was adopted to visualize ChIP-seq tracks, while ChIP-seq heat maps were generated using deepTools (47).

Drug sensitivity analysis. The Genomics of Drug Sensitivity in Cancer (GDSC; https://www.cancerrxgene.org/) database was utilized to evaluate the sensitivity of various chemotherapeutic agents. The pRRophetic package was employed to estimate the IC_{50} of these drugs (48).

Statistical analysis. All experiments were performed in triplicate and repeated three times. All statistical analyses and subsequent visualization were implemented using R software (version 4.1.0). The data were assessed for normal distribution using the Shapiro-Wilk method and for homogeneity of variance using the Levene method. All two-group comparisons of normally distributed data were performed using unpaired Student's t test. For multigroup comparisons, one-way ANOVA with Tukey's post hoc test was used. Data that were not normally distributed or without homogeneity of variance were compared using Kruskal-Wallis with Dunn's post hoc test and Wilcoxon rank sum nonparametric tests. Data are presented as the mean ± SEM (error bars). All survival analyses were conducted using KM analysis, the log-rank test and the Cox proportional hazards model or the two-stage method (49). Pearson's test or Spearman's test was used to analyze the correlation of two variables. P<0.05 was considered to indicate a statistically significant difference.

Results

Upregulation of PAXIP1 in HCC. To ascertain the potential involvement of PAXIP1 in HCC, the transcriptional levels of *PAXIP1* across HCC studies were assessed using HCCDB. Analysis of 11 HCC cohorts from this database demonstrated that *PAXIP1* mRNA was upregulated in HCC tissues compared with adjacent non-tumor tissues (Fig. 1A). A more granular examination of TCGA-LIHC samples using the UALCAN database further demonstrated a marked increase in *PAXIP1* expression compared with that in healthy controls across all tumor grades (Fig. 1B and C). In addition, analysis of subgroups stratified by sex, age and ethnicity indicated that *PAXIP1* expression was higher in patients with HCC compared with healthy controls (Fig. S1A-C). The methylation level of the PAXIP1 promoter region varied across groups based on sex,

A

PAXIP1 expression in HCCDB cohort

Dataset	P-value	Type	No.	Mean	STD	IQR
HCCDB1	3.35×10^{-20}	HCC	100	8.989	0.433	0.531
		Adjacent	97	8.476	0.184	0.232
HCCDB3	3.29×10^{-40}	HCC	268	1.102	0.359	0.432
		Adjacent	243	0.741	0.150	0.163
		Cirrhotic	40	0.824	0.156	0.194
		Healthy	6	0.771	0.096	0.062
HCCDB4	4.35×10^{-44}	HCC	240	6.784	0.403	0.618
		Adjacent	193	6.303	0.212	0.275
HCCDB6	2.90×10^{-46}	HCC	225	5.818	0.694	0.937
		Adjacent	220	4.925	0.414	0.491
HCCDB11	0.2553	HCC	88	6.894	0.994	1.534
		Adjacent	48	6.690	0.996	1.711
HCCDB12	4.33×10^{-8}	HCC	81	9.766	0.463	0.685
		Adjacent	80	9.423	0.255	0.319
HCCDB13	4.26×10^{-38}	HCC	228	7.153	0.514	0.634
		Adjacent	168	6.542	0.326	0.380
HCCDB15	3.63×10^{-14}	HCC	351	8.180	0.666	0.805
		Adjacent	49	7.713	0.293	0.390
HCCDB16	1.65×10^{-8}	HCC	60	7.843	0.371	0.508
		Adjacent	60	7.501	0.214	0.139
HCCDB17	1.17×10^{-12}	HCC	115	8.236	0.338	0.485
		Adjacent	52	7.891	0.223	0.203
HCCDB18	2.44×10^{-49}	HCC	212	2.381	0.433	0.620
		Adjacent	177	1.764	0.256	0.300

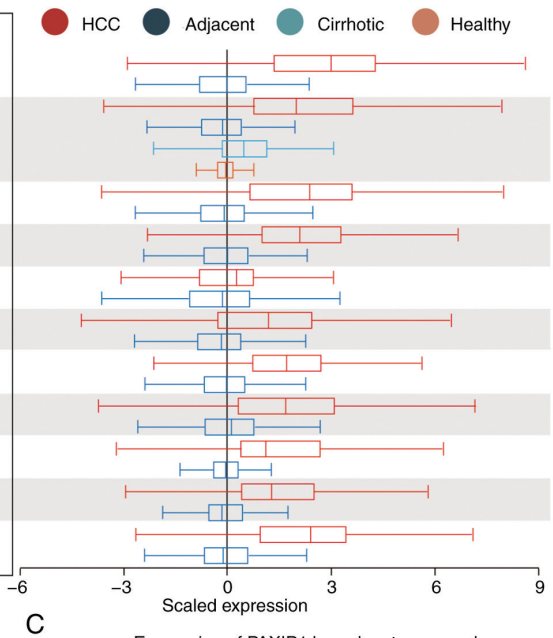

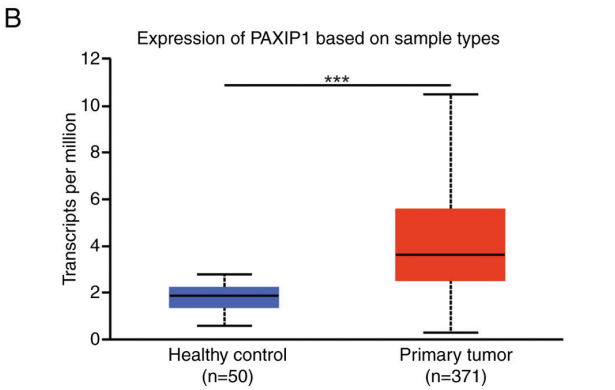

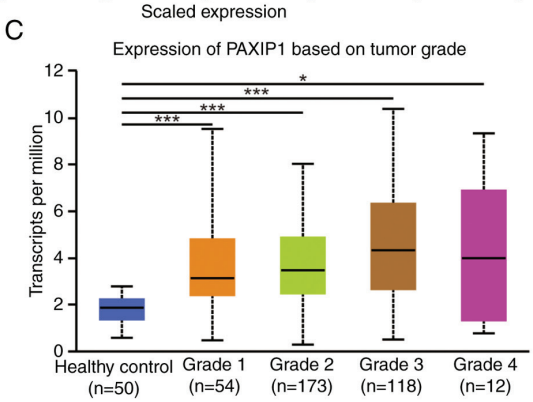

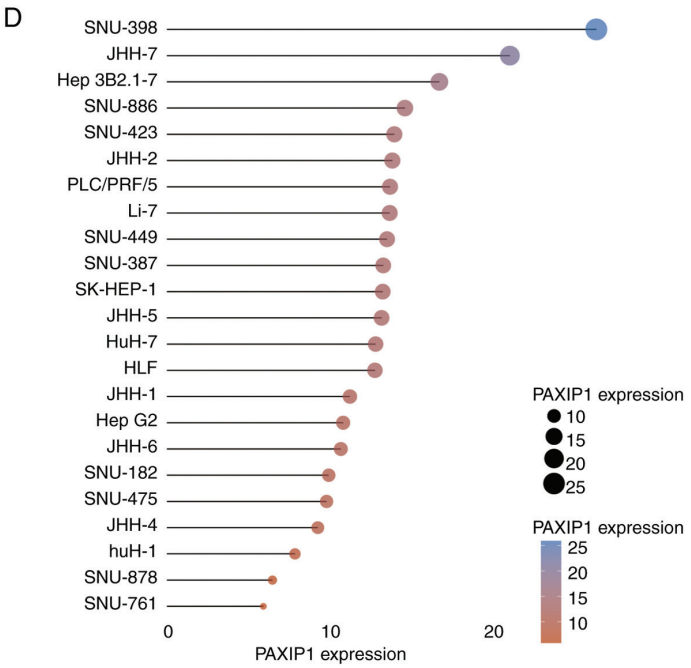

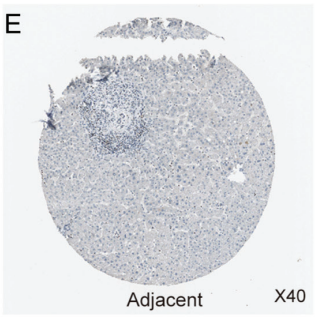

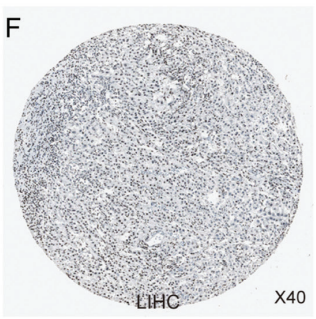

Figure 1. Increased PAXIP1 expression in HCC. (A) Expression levels of PAXIP1 in tumor tissues vs. adjacent non-tumor tissues in HCCDB, as analyzed using an unpaired Student's t-test. For HCCDB3, tumor tissues were compared with adjacent non-tumor tissues using an unpaired Student's t-test. The sample sizes (n) were as indicated. Boxplots illustrating the relative expression levels of PAXIP1 in healthy controls and HCC samples based on (B) sample types and (C) tumor grade in The Cancer Genome Atlas. (B) Unpaired two-tailed Student's t-test. ***P<0.001. (C) One-way ANOVA. *P<0.05, ***P<0.001. The sample sizes (n) were as indicated. (D) Analysis of the expression profile of PAXIP1 mRNA across 23 distinct HCC cell lines based on the Cancer Cell Line Encyclopedia database. Protein expression levels of PAXIP1 according to immunohistochemical staining (HPA006694) in (E) adjacent non-tumor tissues and (F) LIHC tissues from the HPA database. Magnification, x40. HCC, hepatocellular carcinoma; HCCDB, Integrative Molecular Database of HCC; HPA, Human Protein Atlas; IQR, interquartile range; LIHC, liver hepatocellular carcinoma; PAXIP1, PAX-interacting protein 1; STD, standard deviation.

age and ethnicity (Fig. S1D-F). The mRNA expression matrix from the Cancer Cell Line Encyclopedia dataset corroborated these findings, showing that PAXIP1 was highly expressed in HCC cell lines (Fig. 1D). Furthermore, immunohistochemical analysis from the HPA database showed an absence of PAXIP1 protein in adjacent non-tumor liver tissues, while its expression was elevated in HCC tumor tissues (Fig. 1E and F). Therefore, the aforementioned results suggested that PAXIP1 expression was upregulated in HCC.

High PAXIP1 expression is associated with poor prognosis in patients with HCC. To elucidate the relationship between *PAXIP1* expression and HCC prognosis, *PAXIP1* genomic alterations were first analyzed in HCC using the cBioPortal website. The results showed that genomic alterations in *PAXIP1* were present in 1.2% of patients (Fig. 2A). These alterations were diverse in nature (Fig. 2B). Among patients with HCC, amplification was one of the major types of *PAXIP1* copy number variation (Fig. 2C). The prognostic significance of PAXIP1 expression was further analyzed in HCC. Analysis of the overall survival (OS) rate showed that patients with high PAXIP1 expression had a low survival rate (Fig. 3A). For the receiver operating characteristic (ROC) curves, the AUC value range was 0.66-0.59 for 1-, 3- and 5-year prognoses (Fig. 3B). To determine whether PAXIP1 could be used as an independent prognostic factor, univariate and multivariate Cox regression analyses were performed. Univariate Cox regression analysis indicated that PAXIP1 was a significant risk factor for OS in patients with HCC (Fig. 3C; P=0.03328).

However, further multivariate Cox regression analysis and nomogram results showed that PAXIP1 was not an independent risk factor for HCC (Fig. 3D-F). Collectively, these findings indicated that a high level of PAXIP1 may predict a low survival rate of patients with HCC.

PAXIP1 co-expression networks in HCC. To investigate the biological significance of PAXIP1 in HCC, PAXIP1 co-expression was examined in an HCC cohort using the LinkedOmics function module. It was shown that 5,710 genes were positively correlated with PAXIP1, while 3,317 genes were negatively correlated with PAXIP1 (false discovery rate <0.01; Fig. 4A). The heatmap further illustrates these correlations, highlighting the top 50 most significant genes, which were positively and negatively correlated with PAXIP1 expression (Fig. 4B and C). Subsequent GSEA was conducted to clarify the principal GO terms associated with PAXIP1 co-expressed genes. The analysis of GO biological process categories showed that the genes co-expressed with PAXIP1 were predominantly involved in processes such as 'Protein alkylation', 'Covalent chromatin modification', 'Non-recombinational repair' and 'Maintenance of cell number', whereas 'Mitochondrial respiratory chain complex assembly', 'NADH dehydrogenase complex assembly', 'Translational elongation', 'mitochondrial gene expression' and multiple metabolic processes were found to be downregulated (Fig. 4D; Table SI). KEGG pathway analysis indicated notable enrichment in pathways such as 'MicroRNAs in cancer', 'Cell cycle', 'Complement and coagulation cascades' and 'Metabolism of xenobiotics by cytochrome P450' (Fig. 4E; Table SII). These findings suggested the extensive impact of PAXIP1 on the global transcriptome, highlighting its potential role in HCC pathogenesis.

Functional analysis of PAXIP1 target genes in HCC. PAXIP1 was associated with the survival rate of patients with HCC. Therefore, a functional analysis of PAXIP1 target genes was performed. Using ChIP-seq data, 2,370 target genes were identified based on their binding scores (Table SIII). Using DAVID (26,50) and Metascape (27), functional annotation of the 2,370 PAXIP1 target genes was performed. The most enriched terms in the GO (Fig. 5A) and KEGG (Fig. 5B) analyses are shown. Notably, metabolism-related pathways or processes showed a high frequency of occurrence, including 'Oxocarboxylic acid metabolism', 'Carbon metabolism' and 'Propanoate metabolism', indicating a potential role of PAXIP1 in the metabolic mechanisms during HCC tumorigenesis.

The network of enriched terms elucidated the intricate interactions among the terms with considerable detail (Fig. 5C). To further understand the biological functions of the 2,370 PAXIP1 targets, the Metascape database (https://metascape.org/) was also employed to perform DisGeNET and PaGenBase enrichment analyses. The summary of enrichment analysis in DisGeNET and PaGenBase showed that the differentially expressed genes were mainly enriched in 'Hepatomegaly' (Fig. 5D) and 'liver' (Fig. 5E). These results suggested a tissue- or cell-specific role for PAXIP1 and its target genes in HCC. Therefore, PAXIP1 may be associated with HCC tumorigenesis via dysregulation of multiple pathways.

Special regions in HCC co-occupied by PAXIP1, MYBL2 and FOXO1. To understand the involvement of PAXIP1 in HCC and to expand the investigation to a genomic scale, the binding features of PAXIP1 in HCC cells were examined. By performing co-localization analysis of PAXIP1 ChIP-seq data (GSE104247) derived from HepG2 cells (22), 19 potential genes were identified and a multi-gene summary was performed using HCCDB. These genes were separated into two groups (upregulated and downregulated) based on their expression levels in HCC (Fig. 6A). Analysis using the GEPIA database revealed a marked increase in MYBL2 expression and a notable decrease in FOXO1 expression in HCC (Fig. 6B and C). Notably, FOXO1 expression was not significantly changed when combining TCGA data with Genotype-Tissue Expression data (Fig. 6C).

The genomic distribution of PAXIP1, MYBL2 (GSE32465) and FOXO1 (GSE104247) was then analyzed using data from previous studies (21,22). To visualize the overlap of PAXIP1, MYBL2 and FOXO1 binding sites, chromosomal folding was represented using a Hilbert curve, which preserves the spatial proximity of linearly adjacent regions (51). The distributions of PAXIP1, MYBL2 and FOXO1 exhibited similar patterns at the whole-genome scale (Fig. 6D). It was further revealed that PAXIP1 shares 14,324 peaks with MYBL2 and 6,991 peaks with FOXO1 (Fig. 6E and F). To further analyze the relationship between PAXIP1, MYBL2 and FOXO1, the signals of PAXIP1, MYBL2 and FOXO1 were plotted in descending order in the PAXIP1/MYBL2- and PAXIP1/FOXO1-cobound regions. PAXIP1 occupancy showed a similar pattern with MYBL2 and FOXO1 in their co-bound regions

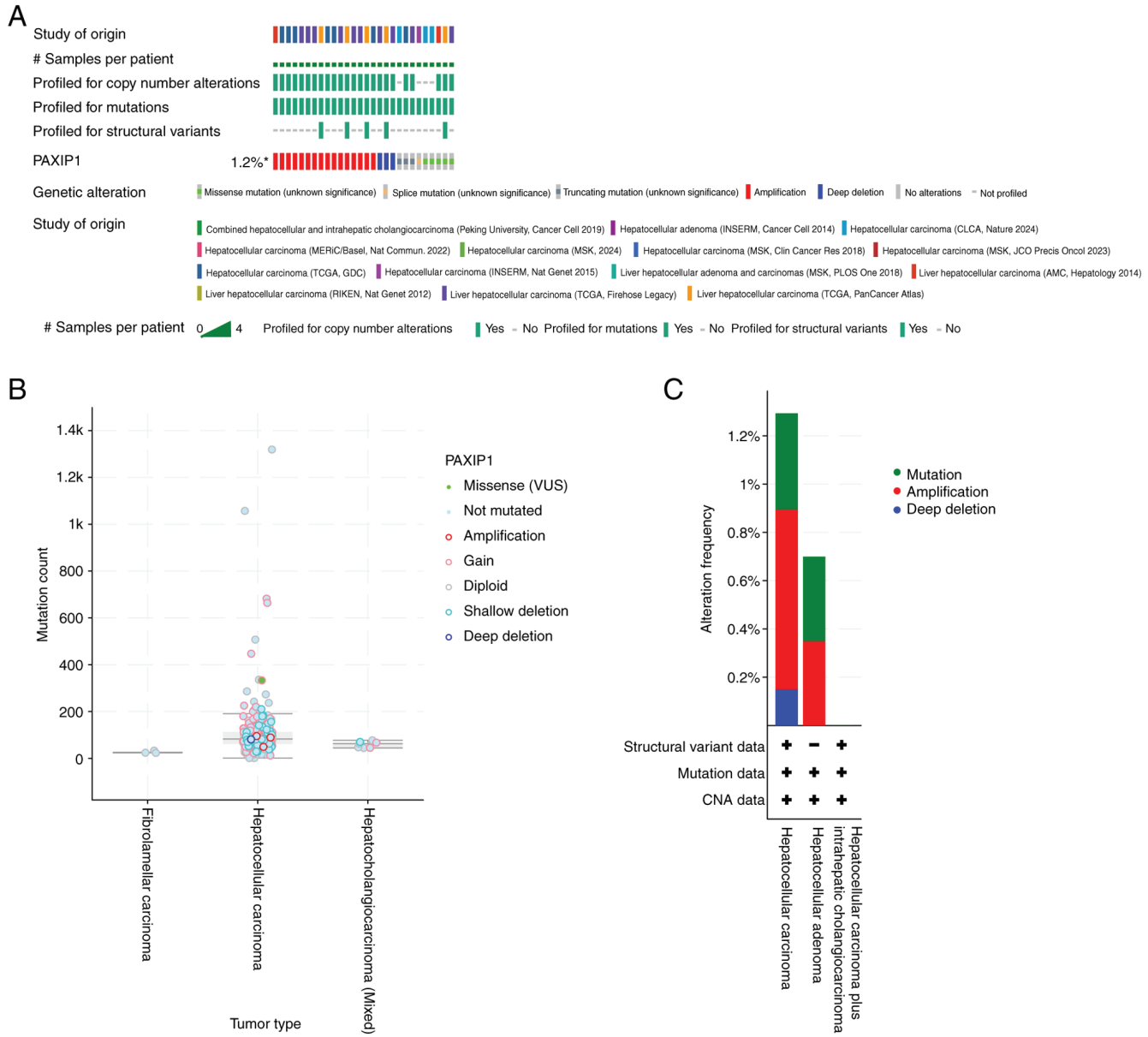

Figure 2. PAXIP1 genomic alterations in fourteen studies of liver carcinomas analyzed using the cBioPortal database. (A) OncoPrint analysis of PAXIP1 gene alterations in cancer cohorts. (B) Diverse alterations of the PAXIP1 gene in cancer cohorts. (C) Characterization of PAXIP1 Gene Alteration Types in Cancer Cohorts. INSERM, French National Institute of Health and Medical Research; CLCA, Chinese Liver Cancer Atlas; MERiC/Basel, Meric Ataman University of Basel; MSK, Memorial Sloan Kettering Cancer Center; TCGA, The Cancer Genome Atlas; AMC, Asan Medical Center; RIKEN, RIKEN Yokohama Japan; N.S., not significant; PAXIP1, PAX-interacting protein 1; VUS, variants of uncertain significance.

(Fig. 6G and H). Survival analysis revealed that in patients with HCC, elevated MYBL2 expression was associated with poorer OS, while reduced FOXO1 expression was also associated with worse OS outcomes. However, only the difference in OS related to MYBL2 expression was statistically significant, whereas the difference associated with FOXO1 expression was not significant (Fig. 6I and J). Taken together, these findings demonstrated that PAXIP1 functioned as a cofactor for MYBL2 or FOXO1 in HCC.

Prediction and analysis of potential TFs of PAXIP1 in HCC. TFs are responsible for regulating gene expression in HCC development (52). To assess whether PAXIP1 was modulated by TFs, the upstream TFs of PAXIP1 were first predicted and the top 10 predicted TFs were identified using the hTF target database (Fig. 7A). Subsequently, survival analysis for all 10 TFs was performed (Figs. 7B, C and S2). Among these TFs, CTCF and NRF1 have been demonstrated to be prognostic markers in liver cancer (53,54), according to the HPA database. No statistically significant differences were found; however, there was a tendency that elevated CTCF and NRF1 expression levels were associated with poorer patient outcomes in HCC (Fig. 7B and C). To confirm the role of NRF1 and CTCF in the regulation of PAXIP1 in HCC, NRF1 and CTCF were knocked down with targeted siRNA. Decreased expression of NRF1 resulted in decreased PAXIP1 expression in HuH-7 and PLC-PRF-5 cells; however, CTCF knockdown did not affect PAXIP1 expression (Fig. 7D). The aforementioned findings suggested that NRF1 may regulate PAXIP1 expression during the development of liver cancer.

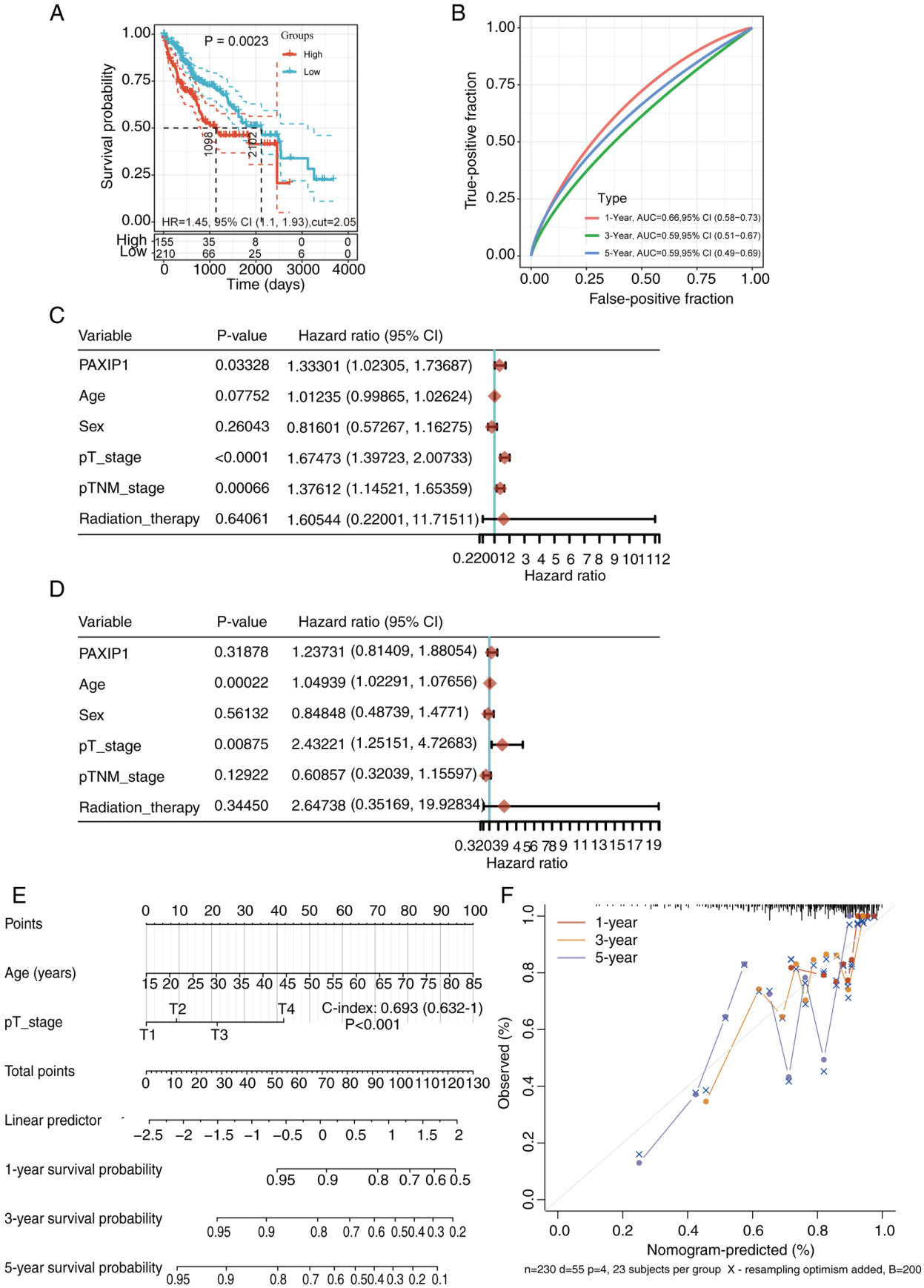

Figure 3. PAXIP1 is associated with survival in HCC. (A) Survival probability of the PAXIP1-high and PAXIP1-low groups. The P-value and HR with the 95% CI were calculated using log-rank tests. The sample sizes (n) were as indicated. (B) Time-dependent receiver operating characteristic curve analysis of PAXIP1 for 1, 3 and 5 years. P-value, risk coefficient (HR) and CI as determined using (C) univariate and (D) multivariate Cox regression analysis. (E) Nomogram for the survival of patients with HCC (1-, 2- and 3-year overall survival). (F) Calibration curve for the overall survival nomogram model in predicting 1-, 3- and 5-year overall survival in patients with HCC. AUC, area under the curve; C-index, concordance index; HCC, hepatocellular carcinoma; HR, hazard ratio; PAXIP1, PAX-interacting protein 1.

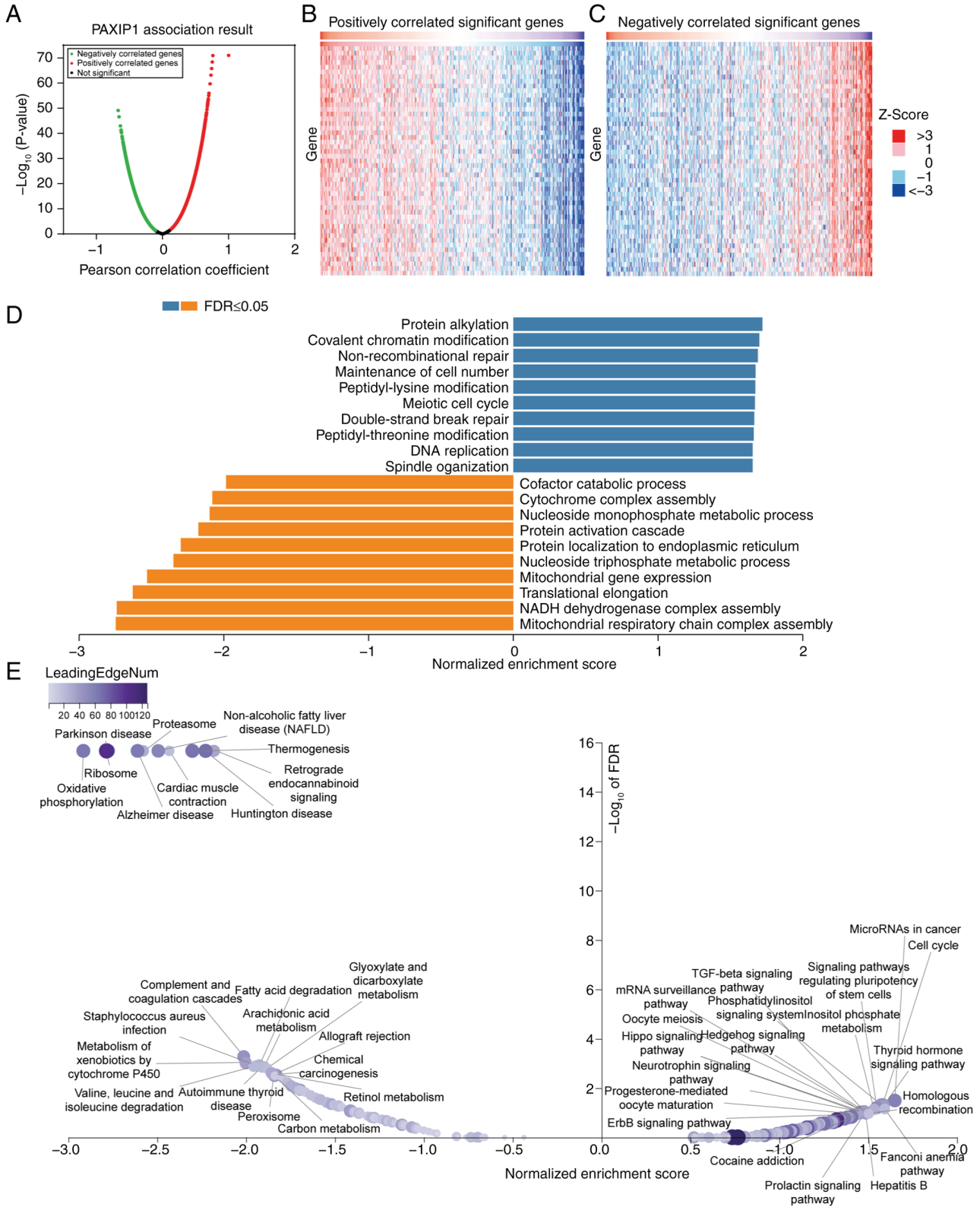

Figure 4. PAXIP1 co-expression genes in HCC analyzed using the LinkedOmics database. (A) Genes associated with PAXIP1 expression were identified using Pearson correlation analysis in the HCC cohort. (B) Heatmap depicting the top 50 genes showing a positive correlation with PAXIP1 in HCC. (C) Heatmap depicting the top 50 genes showing a negative correlation with PAXIP1 in HCC. (D) Gene Ontology biological process terms enriched in PAXIP1-associated genes in the HCC cohort. (E) Kyoto Encyclopedia of Genes and Genomes pathways enriched in PAXIP1-associated genes in the HCC cohort. FDR, false discovery rate; HCC, hepatocellular carcinoma; NAFLD, non-alcoholic fatty liver disease; PAXIP1, PAX-interacting protein 1.

Since potential cofactors and regulators of PAXIP1 were identified, the prognostic significance of these genes in HCC was assessed. Patients with HCC were redivided into the high-risk (n=185) and low-risk groups (n=185) according to the median risk score (Fig. 7E-G). Those in the high-risk group exhibited worse outcomes than

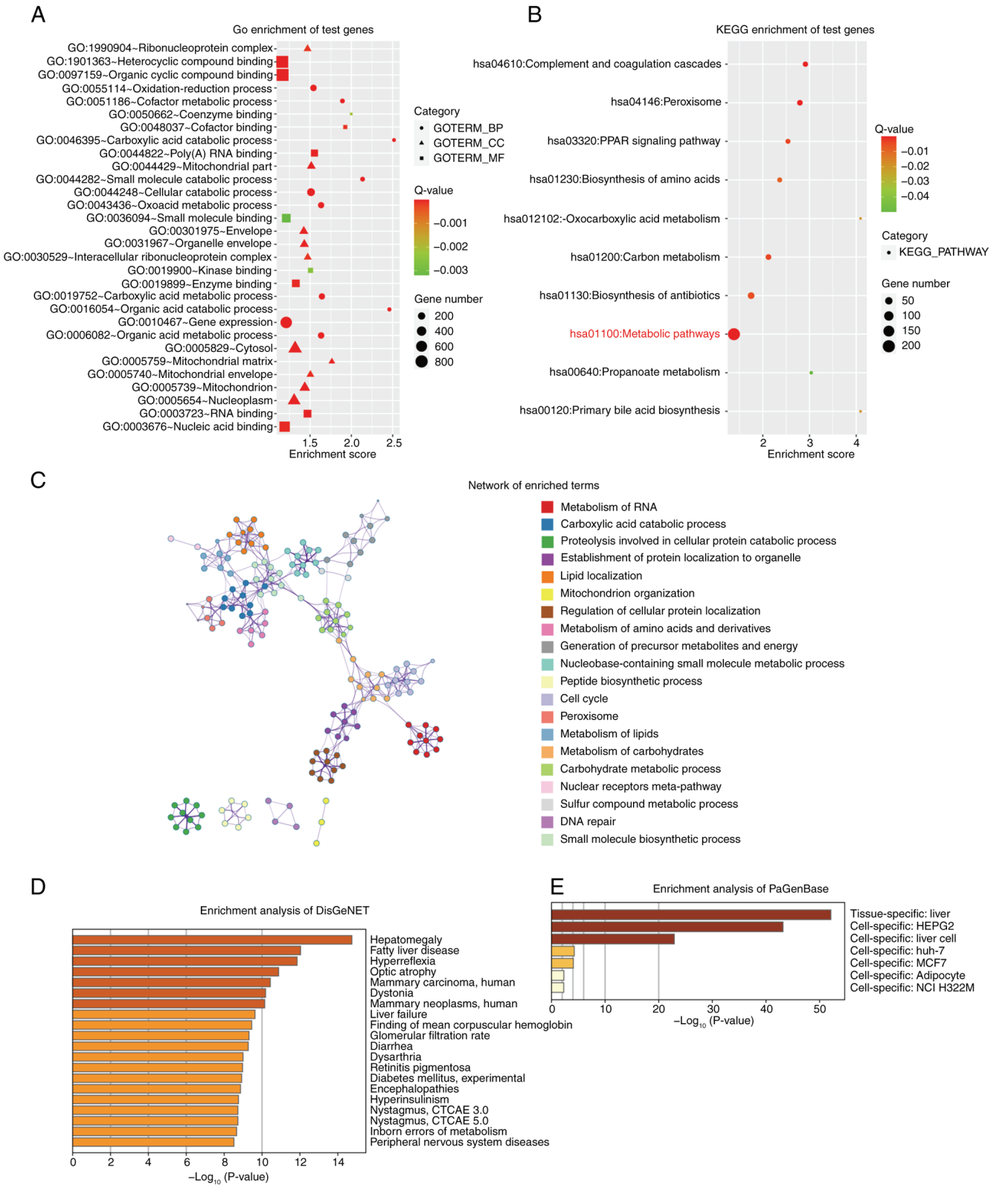

Figure 5. Enrichment analysis of PAXIP1 target genes in the GSE32465 and GSE104247 datasets. (A) Top 10 GO-BP, GO-CC and GO-MF terms enriched in the GO analysis of the HepG2 cell line. (B) Top 10 pathways enriched in the KEGG analysis in HepG2 cells. (C) Metascape network of enriched terms for PAXIP1 target genes. (D) Enrichment analysis of DisGeNET using Metascape. (E) Enrichment analysis of PaGenBase using Metascape. BP, biological process; CC, cellular component; CTCAE, Common Terminology Criteria for Adverse Events; GO, Gene Ontology; HCC, hepatocellular carcinoma; KEGG, Kyoto Encyclopedia of Genes and Genomes; MF, molecular function.

their low-risk counterparts (Fig. 7H). For the ROC curve, the AUC range was 0.735-0.649 for the 1-, 3- and 5-year prognoses (Fig. 7I). The results indicated that the combined expression of four genes, PAXIP1, MYBL2, FOXO1 and NRF1, could serve as an effective prognostic marker for HCC.

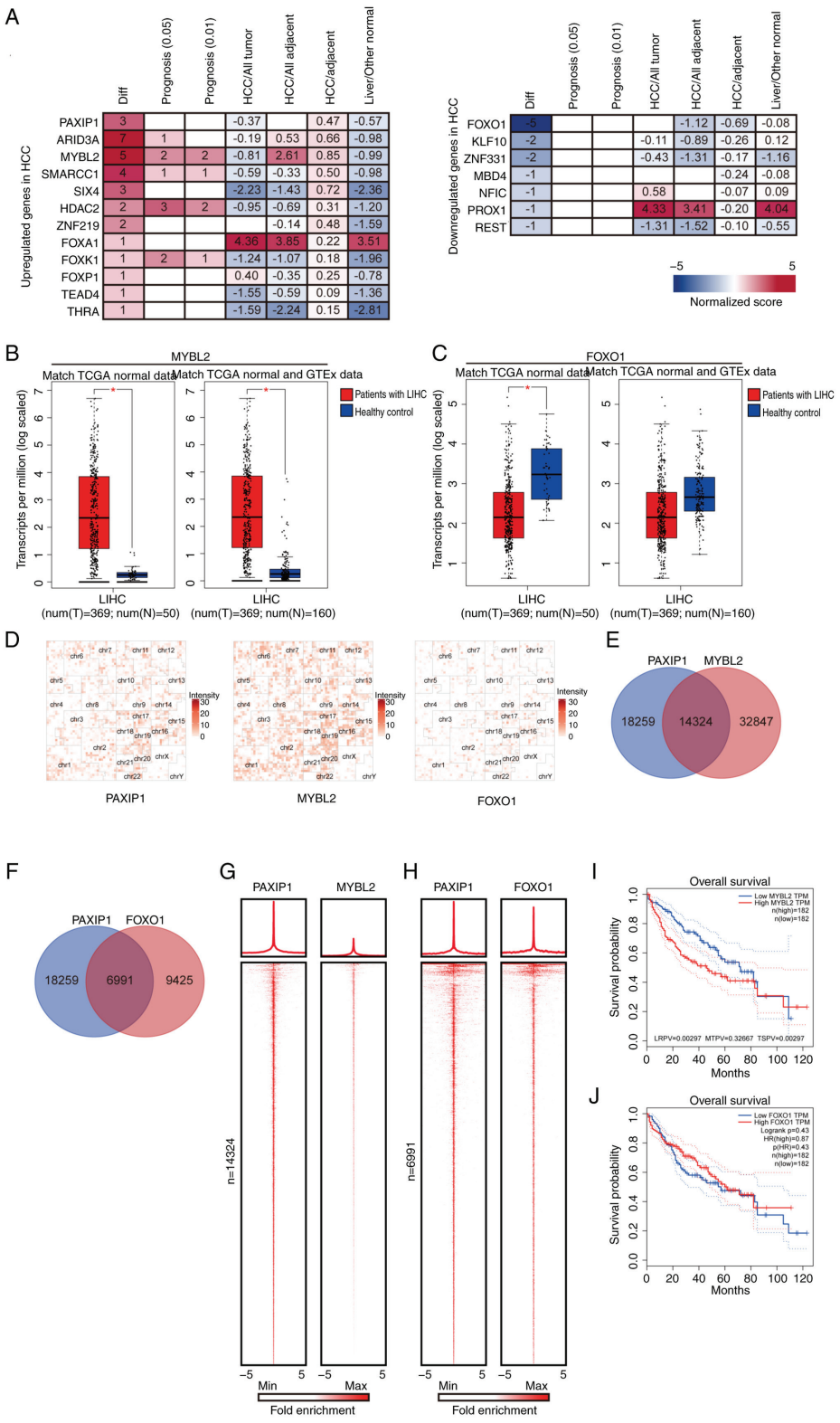

Figure 6. Identification of cofactors of PAXIP1 in HCC. (A) PAXIP1-associated multi-gene summary in the Integrative Molecular Database of HCC. (B) MYBL2 and (C) FOXO1 expression in LIHC tissues compared with corresponding TCGA and GTEx tissues from healthy controls. Unpaired two-tailed Student's t-test. *P<0.01. The sample sizes (n) were as indicated. (D) Hilbert curve plots showing the similarity of distribution of PAXIP1, MYBL2 and FOXO1 in human genomes. (E) Venn diagram showing the overlapping peaks between PAXIP1 and MYBL2. (F) Venn diagram showing the overlapping peaks between PAXIP1 and FOXO1. (G) Average occupancy plots and heatmaps (lower panel) depicting ChIP-seq enrichment patterns for PAXIP1 and MYBL2 within 5 Kb of the center of the PAXIP1 peaks at PAXIP1/MYBL2-cobound regions (n=14,324). (H) Average occupancy plots and heatmaps (lower panel) depicting ChIP-seq enrichment patterns for PAXIP1 and FOXO1 within 5 Kb of the center of the PAXIP1 peaks at PAXIP1/FOXO1-cobound regions (n=6,991). Prognostic value of (I) MYBL2 and (J) FOXO1 in HCC determined using the Gene Expression Profiling Interactive Analysis database. The P-value was calculated using the (I) two-stage method or (J) log-rank test (n=364). ChIP-seq, chromatin immunoprecipitation-sequencing; GTEx, Genotype-Tissue Expression; HCC, hepatocellular carcinoma; HR, hazard ratio; LIHC, liver hepatocellular carcinoma; LRPV, P-value of the log-rank test; MTPV, P-value of the suggested stage-II test; MYBL2, MYB proto-oncogene like 2; N, healthy controls; PAXIP1, PAX-interacting protein 1; T, tumor; TCGA, The Cancer Genome Atlas; TPM, transcripts per million; TSPV, P-value of the two-stage test (TSPV <0.05 represent a statistically significant difference); Diff, number of differentially expressed datasets.

A Top 10 predicted upstream TF of PAXIP1

Gene	TFs	R-value	*P*-value
PAXIP1	CREB1	0.75	8.0×10^{-67}
PAXIP1	CTCF	0.73	7.9×10^{-62}
PAXIP1	ELF1	0.66	3.2×10^{-48}
PAXIP1	GABPA	0.72	7.3×10^{-61}
PAXIP1	NRF1	0.84	7.6×10^{-101}
PAXIP1	REST	0.73	8.3×10^{-63}
PAXIP1	SIN3A	0.77	3.0×10^{-73}
PAXIP1	SP1	0.79	8.1×10^{-79}
PAXIP1	TAF1	0.78	1.5×10^{-75}
PAXIP1	YY1	0.67	7.1×10^{-49}

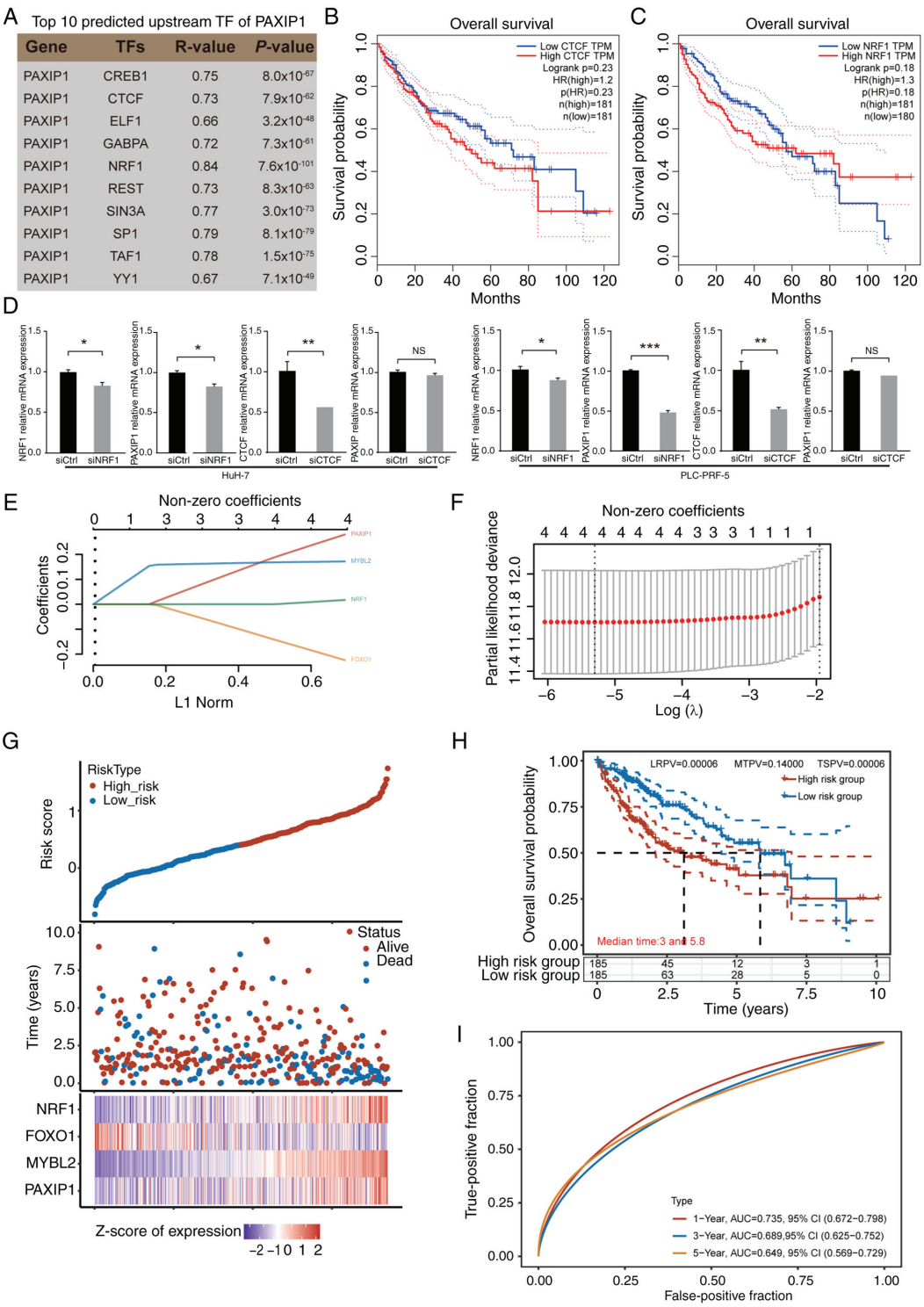

Figure 7. Identification of upstream factors of PAXIP1 in HCC. (A) List of top 10 predicted upstream TFs of PAXIP1. The P-value was calculated using Student's t-test. (B) Overall survival rate of patients with HCC with low and high CTCF expression. The P-value was calculated using the log-rank test (n=362). (C) Overall survival rate of patients with HCC with low and high NRF1 expression. The P-value was calculated using the log-rank test (n=361). (D) Reverse transcription-quantitative PCR analysis demonstrated that NRF1 knockdown downregulated PAXIP1 expression, while CTCF knockdown did not change the expression of PAXIP1 in HCC cells. Mean ± SEM of three independent experiments. Unpaired two-tailed Student's t-test. *P<0.05, **P<0.01, ***P<0.001. (E) Coefficients of PAXIP1, MYBL2, FOXO1 and NRF1 were determined using the lambda parameter. The x-axis represents the lambda values, while the y-axis denotes the coefficients of the independent variables. (F) Relationship between partial likelihood bias and log(λ) plotted through the application of the least absolute shrinkage and selection operator Cox regression model. (G) Risk score, survival time and survival status of selected high-risk and low-risk groups. The top section displays a scatter plot of risk scores arranged from low to high, with different colors representing different risk groups. The middle section shows the scatter plot distribution of risk scores corresponding to survival time and survival status for different samples. The bottom section presents a heatmap of the expression of genes included in the signature. (H) Kaplan-Meier survival analysis was conducted to assess the risk model derived from the dataset, and comparisons between different groups were performed using the two-stage method. (I) Receiver operating characteristic curve and AUC of PAXIP1-related genes. The data in (B, C and E-I) were from The Cancer Genome Atlas. AUC, area under the curve; CTCF, CCCTC binding factor; Ctrl, control; HCC, hepatocellular carcinoma; HR, hazard ratio; LRPV, P-value of the log-rank test; MTPV, P-value of the suggested stage-II test; MYBL2, MYB proto-oncogene like 2; NRF1, nuclear respiratory factor 1; NS, not significant; PAXIP1, PAX-interacting protein 1; si, small interfering RNA; TF, transcription factor; TPM, transcripts per million; TSPV, P-value of the two-stage test.

Relationship between PAXIP1 and tumor immunity in HCC. To elucidate the molecular mechanisms underlying the role of PAXIP1 in HCC, patients were stratified into two subgroups based on PAXIP1 expression levels: i) The PAXIP1-high group (PAXIP1-High; n=186); and ii) the PAXIP1-low group (PAXIP1-Low; n=185), determined by the median expression value. Differential expression analysis between these two subgroups was conducted (Fig. 8A and B). The subsequent GO and KEGG results revealed that the upregulated genes in the PAXIP1-High group were predominantly associated with 'cell cycle' pathways (Fig. 8C), as well as with processes related to 'organelle fission', 'nuclear division' and 'chromosome segregation' (Fig. 8D). Conversely, the downregulated genes in the PAXIP1-High group were involved in 'PPAR signaling pathway', 'metabolism of xenobiotics by cytochrome P450' and 'complement and coagulation cascades' (Fig. 8E), and in 'lipid localization', 'glycerolipid metabolic process' and 'acute inflammatory response' (Fig. 8F). These findings indicated that the differential expression of PAXIP1 target genes may result in the dysregulation of cell division, immune responses and metabolic processes.

The chemotherapeutic response of each sample was assessed using the GDSC database. The 50% maximal inhibitory concentrations for the samples were estimated via ridge regression, and all the involved parameters were set to their default values. To eliminate batch effects, combat normalization was applied, and duplicate gene expression values were summarized by taking their mean. The results showed that the sensitivities to the chemotherapeutic drugs axitinib, lenalidomide, pazopanib, sorafenib and XL-184 (Fig. 9A-E; $P<0.001$) were significantly negatively correlated with PAXIP1 expression in HCC. These analyses indicated that upregulation of PAXIP1 expression may increase sensitivity to the aforementioned chemotherapy drugs in HCC treatment.

Given the possible oncogenic function of PAXIP1 in HCC, it is imperative to explore the relationship between PAXIP1 and immune events in HCC. Utilizing the TIMER database, the correlation between PAXIP1 expression and immune cell infiltration was evaluated. The analysis revealed a positive association between PAXIP1 expression and the presence of $CD4^+$ T cells, neutrophils, macrophages, B cells and myeloid dendritic cells within HCC tissues (Fig. 10A and B). Immune checkpoints such as programmed cell death protein 1 (PD1/PDCD1)/programmed death-ligand 1 (PD-L1/CD274) and cytotoxic T-lymphocyte associated protein 4 (CTLA4) are crucial for the modulation of immune responses and tumor immune evasion (55). The current study demonstrated a significant positive correlation between PAXIP1 expression and the levels of PDCD1, CD274 and CTLA4 (Fig. S3A-C; $P<0.05$). Further analysis using the GEPIA database corroborated these findings, revealing a weak positive correlation between PAXIP1 and PDCD1, CD274 and CTLA4 expression in HCC (Fig. S3D-F). Therefore, PAXIP1 may contribute to carcinogenesis in HCC through mechanisms involving immune cell infiltration and tumor immune escape.

Discussion

HCC is a common and aggressive malignancy found in several countries. A total of 80-90% of liver cancer cases develop because of underlying conditions such as hepatitis B/C virus infection and alcohol-induced liver cirrhosis (56). The exact etiology of liver cancer is under investigation; however, its development originates from a complex interplay of genetic and environmental factors (56). The present study highlighted the significant role of the epigenetic factor PAXIP1 in the pathogenesis and progression of HCC. The results demonstrated that PAXIP1 may be a critical node in HCC development, subject to transcriptional regulation, and may act together with other cofactors to exert its functions. A model of the NRF1-PAXIP1 axis in HCC is shown in Fig. 10C. It was shown that PAXIP1 serves as a prognostic biomarker closely linked to immune infiltration in HCC. This demonstrates that PAXIP1 may be the key in controlling immune cell infiltration, thereby highlighting its potential as a valuable prognostic marker for patients with HCC. Further prospective cohort studies are warranted to elucidate this association, and further research is necessary to identify the prognostic significance of PAXIP1 in HCC.

Research on PAXIP1 as an epigenetic factor has primarily focused on four areas: Developmental biology, DNA damage repair, immune-related functions and tumor development (18,57-62). In 2003, Cho *et al* (13), using PAXIP1 gene knockout mice, found that these mice exhibited delayed development, culminating in embryonic lethality around embryonic day 9.5. Although subsequent analysis revealed that knockout cells were capable of DNA replication, mitotic division was decreased (13). A recent study has also indicated that PAXIP1 is crucial for maintaining mitotic integrity, with PAXIP1 inactivation leading to increased cell death during mitotic exit (57). The results of the present study suggested that PAXIP1 and co-expression genes were involved in multiple processes related to cell division in HCC, including DNA replication and covalent chromatin modifications. PAXIP1 is part of the myeloid/lymphoid or mixed-lineage leukemia 3 (MLL3)/myeloid/lymphoid or mixed-lineage leukemia 4 (MLL4)-complex proteins associated with Set1 (COMPASS)-like complex, which serves a critical role in maintaining DNA modifications and structure (63). These complexes deposit H3K4me1 marks on enhancers to regulate gene transcription (63). The interaction of PAXIP1 with DNA is not solely dependent on the COMPASS-like complex; it also interacts with 53BP1 and participates in DNA damage repair (64).

In the current study, upregulation of PAXIP1 was associated with poor outcomes in patients with HCC. It has been demonstrated that multi-gene prognostic models were more effective and comprehensive than single-gene prognostic models in predicting cancer outcomes (65). FOXK1 (66), FOXO1 (67), histone deacetylase 2 (68), MYBL2 (69) and SWI/SNF related BAF chromatin remodeling complex subunit C1 (70) were previously reported to be favorable or unfavorable prognostic markers in liver cancer, and were associated with PAXIP1 in HCC. The present results were consistent with the aforementioned conclusion. In the present study, using PAXIP1, MYBL2, FOXO1 and NRF1 as a four-gene prognostic marker for HCC had a strong capacity for predicting prognosis.

Metabolic reprogramming is a defining characteristic of numerous cancer types, including HCC. Changes in metabolic processes provide advantages for tumor expansion, tumor

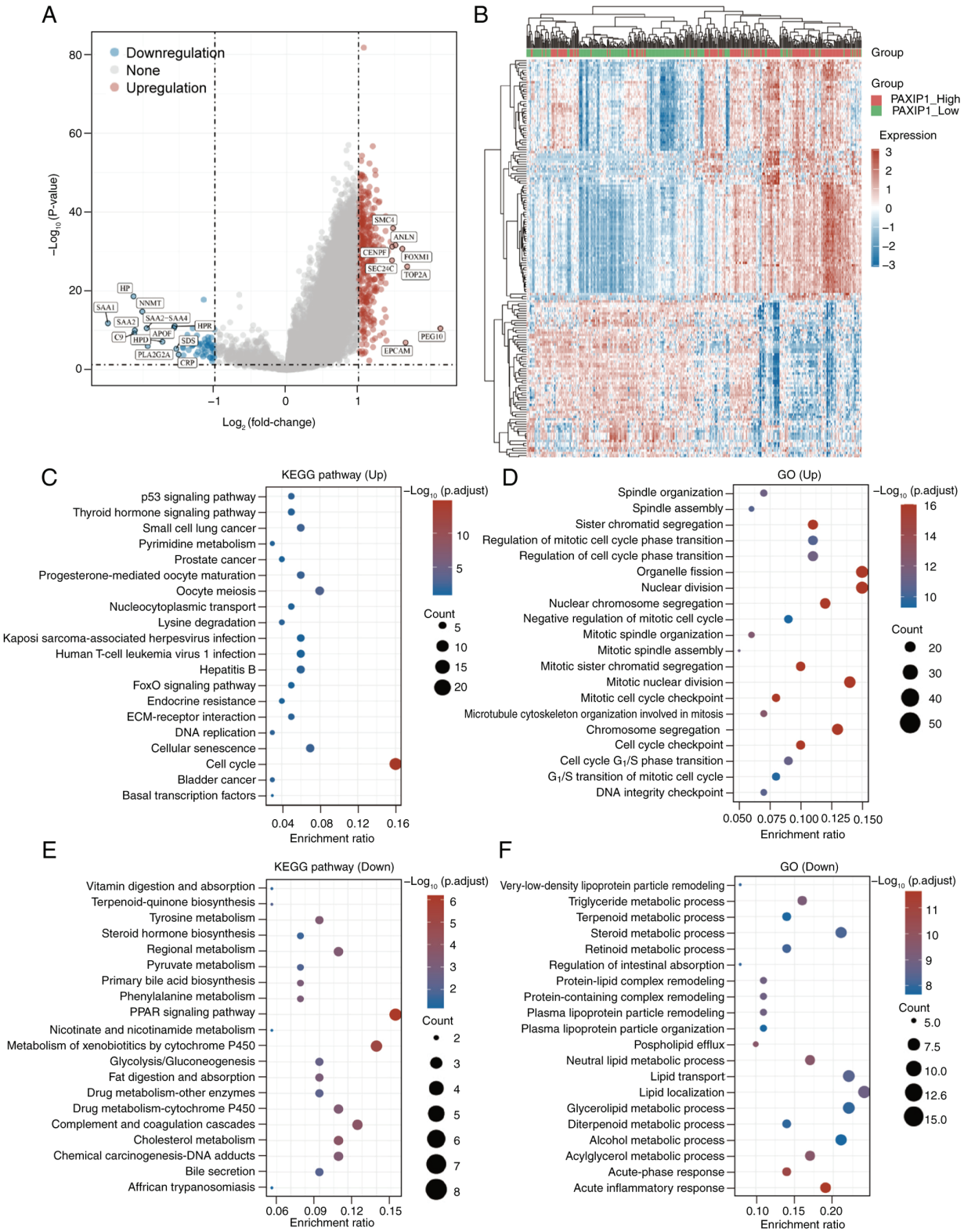

Figure 8. Differential gene expression analysis based on the expression levels of PAXIP1 in hepatocellular carcinoma. (A) Volcano plot indicating upregulated and downregulated genes when comparing PAXIP1-high and PAXIP1-low patients. (B) Heatmap showing the top 50 upregulated genes and top 50 downregulated genes in PAXIP1-high and PAXIP1-low patients. Significantly enriched (C) KEGG pathways and (D) GO annotations of upregulated target genes. Significantly enriched (E) KEGG pathways and (F) GO annotations of downregulated target genes. The data were obtained from The Cancer Genome Atlas. ECM, extracellular matrix; GO, Gene Ontology; KEGG, Kyoto Encyclopedia of Genes and Genomes; p.adjust, adjusted P-value; PAXIP1, PAX-interacting protein 1; PPAR, peroxisome proliferator-activated receptor.

growth and survival by increasing energy production, macromolecular synthesis and redox equilibrium maintenance (71). In the present study, ChIP-seq data were analyzed and it was revealed that PAXIP1 binds to genes associated with metabolism, indicating its potential role in regulating metabolic processes in HCC development. Deficiency of UTX, a

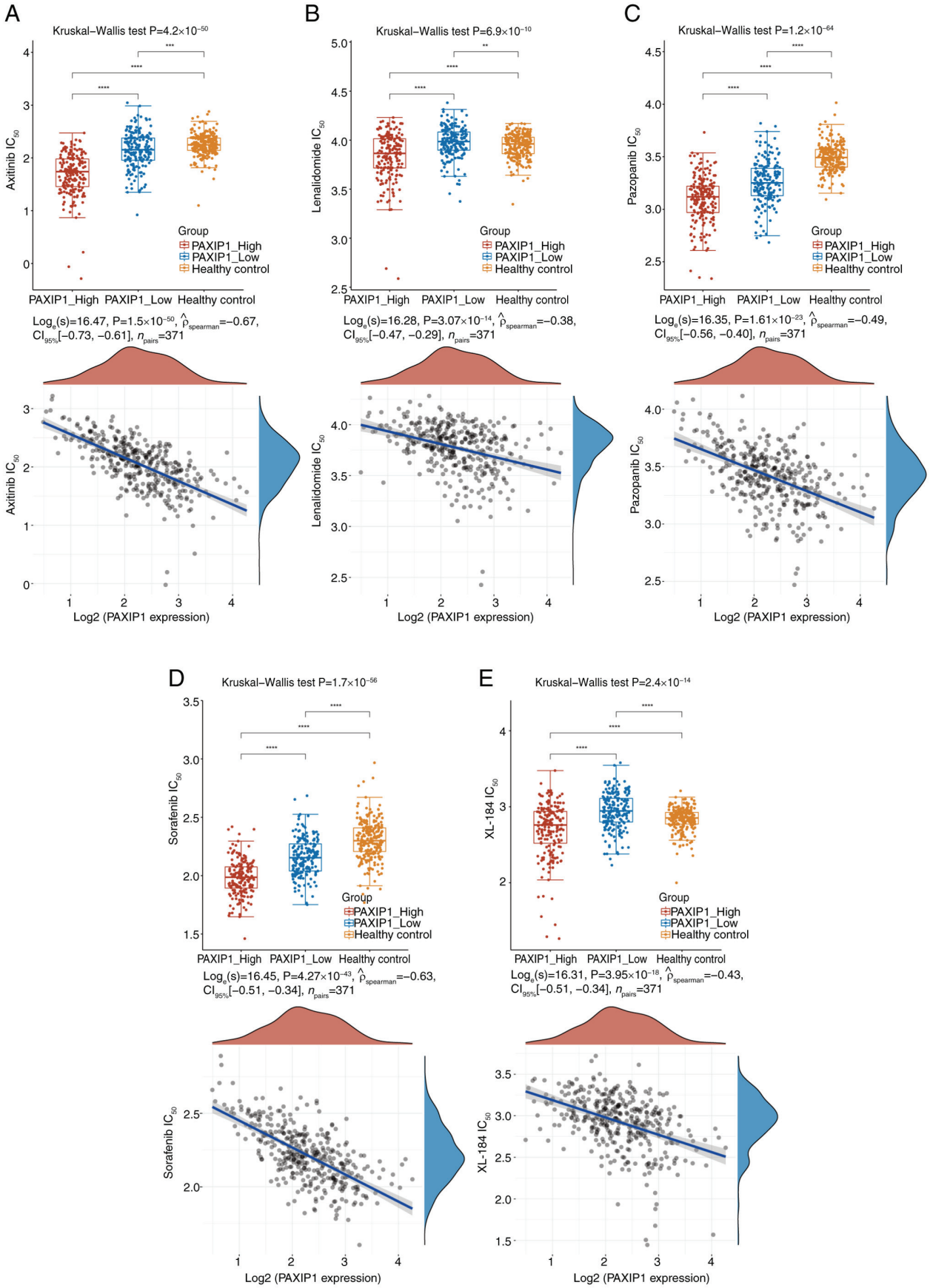

Figure 9. Spearman correlation analysis of the IC_{50} values of compounds from the Genomics of Drug Sensitivity in Cancer database and PAXIP1 gene expression. Distribution of IC_{50} scores, and Spearman correlation analysis of PAXIP1 expression and the IC_{50} of different cancer medicines. (A) Axitinib. (B) Lenalidomide. (C) Pazopanib. (D) Sorafenib. (E) XL-184. For correlation analysis, the horizontal axis illustrates the distribution of PAXIP1 expression levels, while the vertical axis represents the distribution of IC_{50} scores. The density curve on the right represents the trend in the distribution of IC_{50} scores. The density curve at the top represents PAXIP1 expression levels. Kruskal-Wallis test with Dunn's post hoc test. **P<0.01, ***P<0.001, ****P<0.0001. The Spearman correlation coefficient and P-value based on Spearman's test are indicated. The sample sizes (n) were as indicated. PAXIP1, PAX-interacting protein 1.

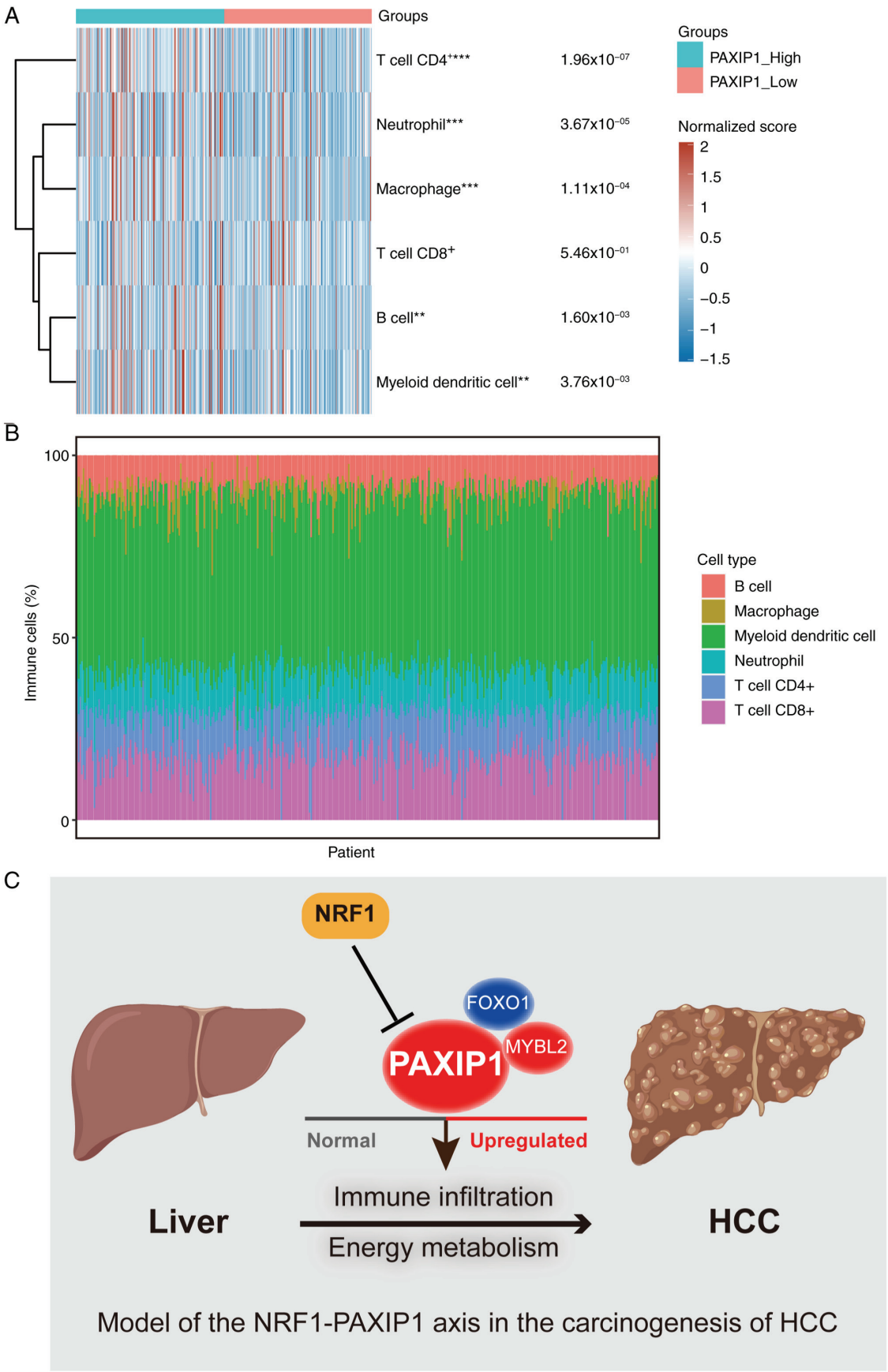

Figure 10. Potential role of PAXIP1 in regulating immune cell infiltration. (A) Heatmap illustrating the correlation between PAXIP1 expression and the extent of immune cell infiltration based on the Tumor Immune Estimation Resource database. Kolmogorov-Smirnov and Wilcoxon rank sum tests. The P-value represents the comparison between PAXIP1-high group and PAXIP1-low group. **P<0.01, ***P<0.001. (B) Heatmap analysis revealed a positive correlation between PAXIP1 expression and various immune cells, including $CD4^+$ T cells, neutrophils, macrophages, B cells and myeloid dendritic cells in HCC. (C) Proposed model of the role of the NRF1-PAXIP1 axis in the carcinogenesis of HCC. HCC, hepatocellular carcinoma; MYBL2, MYB proto-oncogene like 2; NRF1, nuclear respiratory factor 1; PAXIP1, PAX-interacting protein 1.

PAXIP1-interacting protein, in adipocytes leads to metabolic dysfunction in the liver (72). Further evidence is needed to clarify whether UTX is required for PAXIP1 to affect liver cancer metabolism.

Our previous study in *Drosophila* suggested that PAXIP1 mediated a molecular switch between histone modifications, namely H3K4me3/H3K27ac and H3K27me3, in Trithorax-related or polycomb-occupied regions (59). However, to the best of our knowledge, the precise mechanism by which PAXIP1 is specifically recruited to the promoter regions of target genes is yet to be understood. Typically, PAXIP1 specifically binds to target genes through interaction with other specific TFs and recruits them to the promoter region (5). Our previous study indicated that PAXIP1 interacted with Fosl2 or YY1 to be recruited to the EphA2 promoter region in esophageal squamous cell carcinoma (18). The present analysis revealed that PAXIP1, MYBL2 and FOXO1 exhibited similar genomic distributions, and the expression levels of these factors were associated with survival rates in HCC except for those of FOXO1. Therefore, PAXIP1 may be recruited to the promoter regions of its target genes via MYBL2 or FOXO1 in HCC cells.

A pharmacological screen involving 17 kinases found that PAXIP1 enhanced sensitivity to AZD1775 in combination with platinum-based treatment in lung cancer (17). Consistent with a previous study (17), elevated PAXIP1 expression was associated with heightened sensitivity of hepatocellular carcinoma to chemotherapeutic drugs. Further studies are needed to explore the mechanisms underlying the observed associations.

PAXIP1 serves a crucial yet inadequately understood role within the immune system. PAXIP1 participates in immunoglobulin class switching and variable-diversity-joining rearrangement recombination, which depend on MLL3-MLL4 complex activity (73). Another study demonstrated that PAXIP1 regulated thymocyte development in the thymus (74). In Paxip1 knockout mice, a marked increase the population of $CD4^+$ and $CD8^+$ single-positive T cells was observed compared with that in wild-type mice (74). The present analysis revealed a positive association between the expression of PAXIP1 and various immune cell types within the tumor microenvironment, including $CD4^+$ T cells, neutrophils, macrophages, B cells and myeloid dendritic cells. Studies have shown that the infiltration of $CD4^+$ T cells, especially certain subsets such as regulatory T cells and effector memory T cells, is associated with the immune response in HCC (75,76). The results of the present study suggested that PAXIP1 may be implicated in the tumor immune response, potentially offering novel insights for HCC treatment. Overall, the results of the present study revealed a key role of PAXIP1 in HCC development, and provided a novel index for the clinical diagnosis of HCC.

Acknowledgements

Not applicable.

Funding

The present study was supported by grants from the Natural Science Foundation of China (grant nos. 31301146, 82203738 and 82102969), Jiangsu Funding Program for Excellent Postdoctoral Talent (grant no. 2023ZB782), Jiangsu Provincial Medical Key Discipline Cultivation Unit (grant no. JSDW202233) and Huai'an Natural Science Research Program (grant nos. HAB202110 and HAB202101).

Availability of data and materials

The data generated in the present study may be requested from the corresponding author.

Authors' contributions

QC, XH and CWZ conceived the study and revised the manuscript. XH, HX, YLL, FW, XYC and CJ were responsible for data collection, as well as the subsequent data analysis. QC, XH and CWZ confirm the authenticity of all the raw data. QC and CWZ wrote the manuscript. All authors participated in the manuscript development. All authors have read and approved the final version of the manuscript.

Ethics approval and consent to participate

Not applicable.

Patient consent for publication

Not applicable.

Competing interests

The authors declare that they have no competing interests.

References

1. Bray F, Ferlay J, Soerjomataram I, Siegel RL, Torre LA and Jemal A: Global cancer statistics 2018: GLOBOCAN estimates of incidence and mortality worldwide for 36 cancers in 185 countries. CA Cancer J Clin 68: 394-424, 2018.
2. Luo Z, Lu L, Tang Q, Wei W, Chen P, Chen Y, Pu J and Wang J: CircCAMSAP1 promotes hepatocellular carcinoma progression through miR-1294/GRAMD1A pathway. J Cell Mol Med 25: 3793-3802, 2021.
3. Forner A, Llovet JM and Bruix J: Hepatocellular carcinoma. Lancet 379: 1245-1255, 2012.
4. DiStefano JK and Davis B: Diagnostic and prognostic Potential of AKR1B10 in human hepatocellular carcinoma. Cancers (Basel) 11: 486, 2019.
5. Lechner MS, Levitan I and Dressler GR: PTIP, a novel BRCT domain-containing protein interacts with Pax2 and is associated with active chromatin. Nucleic Acids Res 28: 2741-2751, 2000.
6. Shimizu K, Bourillot PY, Nielsen SJ, Zorn AM and Gurdon JB: Swift is a novel BRCT domain coactivator of Smad2 in transforming growth factor beta signaling. Mol Cell Biol 21: 3901-3912, 2001.
7. Cho YW, Hong T, Hong S, Guo H, Yu H, Kim D, Guszczynski T, Dressler GR, Copeland TD, Kalkum M and Ge K: PTIP associates with MLL3- and MLL4-containing histone H3 lysine 4 methyltransferase complex. J Biol Chem 282: 20395-20406, 2007.
8. Munoz IM, Jowsey PA, Toth R and Rouse J: Phospho-epitope binding by the BRCT domains of hPTIP controls multiple aspects of the cellular response to DNA damage. Nucleic Acids Res 35: 5312-5322, 2007.
9. Patel SR, Kim D, Levitan I and Dressler GR: The BRCT-domain containing protein PTIP links PAX2 to a histone H3, lysine 4 methyltransferase complex. Dev Cell 13: 580-592, 2007.
10. Escribano-Diaz C and Durocher D: DNA repair pathway choice-a PTIP of the hat to 53BP1. EMBO Rep 14: 665-666, 2013.

11. Issaeva I, Zonis Y, Rozovskaia T, Orlovsky K, Croce CM, Nakamura T, Mazo A, Eisenbach L and Canaani E: Knockdown of ALR (MLL2) reveals ALR target genes and leads to alterations in cell adhesion and growth. Mol Cell Biol 27: 1889-1903, 2007.
12. Mohan M, Herz HM, Smith ER, Zhang Y, Jackson J, Washburn MP, Florens L, Eissenberg JC and Shilatifard A: The COMPASS family of H3K4 methylases in Drosophila. Mol Cell Biol 31: 4310-4318, 2011.
13. Cho EA, Prindle MJ and Dressler GR: BRCT domain-containing protein PTIP is essential for progression through mitosis. Mol Cell Biol 23: 1666-1673, 2003.
14. Ray Chaudhuri A, Callen E, Ding X, Gogola E, Duarte AA, Lee JE, Wong N, Lafarga V, Calvo JA, Panzarino NJ, *et al*: Replication fork stability confers chemoresistance in BRCA-deficient cells. Nature 535: 382-387, 2016.
15. Willis S, Villalobos VM, Gevaert O, Abramovitz M, Williams C, Sikic BI and Leyland-Jones B: Single gene prognostic biomarkers in ovarian cancer: A meta-analysis. PLoS One 11: e0149183, 2016.
16. De Gregoriis G, Ramos JA, Fernandes PV, Vignal GM, Brianese RC, Carraro DM, Monteiro AN, Struchiner CJ, Suarez-Kurtz G, Vianna-Jorge R and de Carvalho MA: DNA repair genes PAXIP1 and TP53BP1 expression is associated with breast cancer prognosis. Cancer Biol Ther 18: 439-449, 2017.
17. Jhuraney A, Woods NT, Wright G, Rix L, Kinose F, Kroeger JL, Remily-Wood E, Cress WD, Koomen JM, Brantley SG, *et al*: PAXIP1 potentiates the combination of WEE1 inhibitor AZD1775 and platinum agents in lung cancer. Mol Cancer Ther 15: 1669-1681, 2016.
18. Han X, Zhu Y, Shen L, Zhou Y, Pang L, Zhou W, Gu H, Han K, Yang Y, Jiang C, *et al*: PTIP inhibits cell invasion in esophageal squamous cell carcinoma via modulation of EphA2 expression. Front Oncol 11: 629916, 2021.
19. Harland LTG, Simon CS, Senft AD, Costello I, Greder L, Imaz-Rosshandler I, Göttgens B, Marioni JC, Bikoff EK, Porcher C, *et al*: The T-box transcription factor Eomesodermin governs haemogenic competence of yolk sac mesodermal progenitors. Nat Cell Biol 23: 61-74, 2021.
20. Livak KJ and Schmittgen TD: Analysis of relative gene expression data using real-time quantitative PCR and the 2(-Delta Delta C(T)) method. Methods 25: 402-408, 2001.
21. Gertz J, Savic D, Varley KE, Partridge EC, Safi A, Jain P, Cooper GM, Reddy TE, Crawford GE and Myers RM: Distinct properties of cell-type-specific and shared transcription factor binding sites. Mol Cell 52: 25-36, 2013.
22. Partridge EC, Chhetri SB, Prokop JW, Ramaker RC, Jansen CS, Goh ST, Mackiewicz M, Newberry KM, Brandsmeier LA, Meadows SK, *et al*: Occupancy maps of 208 chromatin-associated proteins in one human cell type. Nature 583: 720-728, 2020.
23. Quinlan AR and Hall IM: BEDTools: A flexible suite of utilities for comparing genomic features. Bioinformatics 26: 841-842, 2010.
24. Ramirez F, Ryan DP, Grüning B, Bhardwaj V, Kilpert F, Richter AS, Heyne S, Dündar F and Manke T: deepTools2: A next generation web server for deep-sequencing data analysis. Nucleic Acids Res 44 (W1): W160-W165, 2016.
25. Yu G, Wang LG and He QY: ChIPseeker: An R/Bioconductor package for ChIP peak annotation, comparison and visualization. Bioinformatics 31: 2382-2383, 2015.
26. Huang da W, Sherman BT and Lempicki RA: Systematic and integrative analysis of large gene lists using DAVID bioinformatics resources. Nat Protoc 4: 44-57, 2009.
27. Zhou Y, Zhou B, Pache L, Chang M, Khodabakhshi AH, Tanaseichuk O, Benner C and Chanda SK: Metascape provides a biologist-oriented resource for the analysis of systems-level datasets. Nat Commun 10: 1523, 2019.
28. Lian Q, Wang S, Zhang G, Wang D, Luo G, Tang J, Chen L and Gu J: HCCDB: A database of hepatocellular carcinoma expression atlas. Genomics Proteomics Bioinformatics 16: 269-275, 2018.
29. Riillo C, Polerà N, Di Martino MT, Juli G, Hokanson CA, Odineca T, Signorelli S, Grillone K, Ascrizzi S and Mancuso A, *et al*: A pronectin™ AXL-targeted first-in-class bispecific T cell engager (pAXLxCD3ε) for ovarian cancer. J Transl Med 21: 301, 2023.
30. Thul PJ and Lindskog C: The human protein atlas: A spatial map of the human proteome. Protein Sci 27: 233-244, 2018.
31. Cerami E, Gao J, Dogrusoz U, Gross BE, Sumer SO, Aksoy BA, Jacobsen A, Byrne CJ, Heuer ML, Larsson E, *et al*: The cBio cancer genomics portal: An open platform for exploring multidimensional cancer genomics data. Cancer Discov 2: 401-404, 2012.
32. de Bruijn I, Kundra R, Mastrogiacomo B, Tran TN, Sikina L, Mazor T, Li X, Ochoa A, Zhao G, Lai B, *et al*: Analysis and visualization of longitudinal genomic and clinical data from the AACR project GENIE biopharma collaborative in cBioPortal. Cancer Res 83: 3861-3867, 2023.
33. Xue R, Chen L, Zhang C, Fujita M, Li R, Yan SM, Ong CK, Liao X, Gao Q, Sasagawa S, *et al*: Genomic and transcriptomic profiling of combined hepatocellular and intrahepatic cholangiocarcinoma reveals distinct molecular subtypes. Cancer Cell 35: 932-947.e8, 2019.
34. Chen L, Zhang C, Xue R, Liu M, Bai J, Bao J, Wang Y, Jiang N, Li Z, Wang W, *et al*: Deep whole-genome analysis of 494 hepatocellular carcinomas. Nature 627: 586-593, 2024.
35. Ng CKY, Dazert E, Boldanova T, Coto-Llerena M, Nuciforo S, Ercan C, Suslov A, Meier MA, Bock T, Schmidt A, *et al*: Integrative proteogenomic characterization of hepatocellular carcinoma across etiologies and stages. Nat Commun 13: 2436, 2022.
36. Harding JJ, Nandakumar S, Armenia J, Khalil DN, Albano M, Ly M, Shia J, Hechtman JF, Kundra R, El Dika I, *et al*: Prospective genotyping of hepatocellular carcinoma: Clinical implications of next-generation sequencing for matching patients to targeted and immune therapies. Clin Cancer Res 25: 2116-2126, 2019.
37. Cowzer D, White JB, Chou JF, Chen PJ, Kim TH, Khalil DN, El Dika IH, Columna K, Yaqubie A, Light JS, *et al*: Targeted molecular profiling of circulating cell-free DNA in patients with advanced hepatocellular carcinoma. JCO Precis Oncol 7: e2300272, 2023.
38. Schulze K, Imbeaud S, Letouzé E, Alexandrov LB, Calderaro J, Rebouissou S, Couchy G, Meiller C, Shinde J, Soysouvanh F, *et al*: Exome sequencing of hepatocellular carcinomas identifies new mutational signatures and potential therapeutic targets. Nat Genet 47: 505-511, 2015.
39. Zheng J, Sadot E, Vigidal JA, Klimstra DS, Balachandran VP, Kingham TP, Allen PJ, D'Angelica MI, DeMatteo RP, Jarnagin WR and Ventura A: Characterization of hepatocellular adenoma and carcinoma using microRNA profiling and targeted gene sequencing. PLoS One 13: e0200776, 2018.
40. Ahn SM, Jang SJ, Shim JH, Kim D, Hong SM, Sung CO, Baek D, Haq F, Ansari AA, Lee SY, *et al*: Genomic portrait of resectable hepatocellular carcinomas: Implications of RB1 and FGF19 aberrations for patient stratification. Hepatology 60: 1972-1982, 2014.
41. Fujimoto A, Totoki Y, Abe T, Boroevich KA, Hosoda F, Nguyen HH, Aoki M, Hosono N, Kubo M, Miya F, *et al*: Whole-genome sequencing of liver cancers identifies etiological influences on mutation patterns and recurrent mutations in chromatin regulators. Nat Genet 44: 760-764, 2012.
42. Pilati C, Letouzé E, Nault JC, Imbeaud S, Boulai A, Calderaro J, Poussin K, Franconi A, Couchy G, Morcrette G, *et al*: Genomic profiling of hepatocellular adenomas reveals recurrent FRK-activating mutations and the mechanisms of malignant transformation. Cancer Cell 25: 428-441, 2014.
43. Vasaikar SV, Straub P, Wang J and Zhang B: LinkedOmics: Analyzing multi-omics data within and across 32 cancer types. Nucleic Acids Res 46 (D1): D956-D963, 2018.
44. Chen Y, Li B, Wang J, Liu J, Wang Z, Mao Y, Liu S, Liao X and Chen J: Identification and verification of the prognostic value of the glutathione S-transferase Mu genes in gastric cancer. Oncol Lett 20: 100, 2020.
45. Zhang Z, Lin E, Zhuang H, Xie L, Feng X, Liu J and Yu Y: Construction of a novel gene-based model for prognosis prediction of clear cell renal cell carcinoma. Cancer Cell Int 20: 27, 2020.
46. Zhang Q, Liu W, Zhang HM, Xie GY, Miao YR, Xia M and Guo AY: hTFtarget: A comprehensive database for regulations of human transcription factors and their targets. Genomics Proteomics Bioinformatics 18: 120-128, 2020.
47. Thorvaldsdóttir H, Robinson JT and Mesirov JP: Integrative genomics viewer (IGV): High-performance genomics data visualization and exploration. Brief Bioinform 14: 178-192, 2013.
48. Geeleher P, Cox N and Huang RS: pRRophetic: An R package for prediction of clinical chemotherapeutic response from tumor gene expression levels. PLoS One 9: e107468, 2014.

49. Li H, Han D, Hou Y, Chen H and Chen Z: Statistical inference methods for two crossing survival curves: A comparison of methods. PLoS One 10: e0116774, 2015.
50. Huang da W, Sherman BT and Lempicki RA: Bioinformatics enrichment tools: Paths toward the comprehensive functional analysis of large gene lists. Nucleic Acids Res 37: 1-13, 2009.
51. Anders S: Visualization of genomic data with the Hilbert curve. Bioinformatics 25: 1231-1235, 2009.
52. Goodall GJ and Wickramasinghe VO: RNA in cancer. Nat Rev Cancer 21: 22-36, 2021.
53. Shetron SG: Large-scale ecosystem restoration: Five case studies from the United States. Choice: Current Reviews for Academic Libraries 46: 715-716, 2008.
54. Wang Y, Guo X, Niu Z, Huang X, Wang B and Gao L: DeepCBS: Shedding light on the impact of mutations occurring at CTCF binding sites. Front Genet 15: 1354208, 2024.
55. Srinivasan P, Wu X, Basu M, Rossi C and Sandler AD: PD-L1 checkpoint inhibition and anti-CTLA-4 whole tumor cell vaccination counter adaptive immune resistance: A mouse neuroblastoma model that mimics human disease. PLoS Med 15: e1002497, 2018.
56. Yang JD, Hainaut P, Gores GJ, Amadou A, Plymoth A and Roberts LR: A global view of hepatocellular carcinoma: Trends, risk, prevention and management. Nat Rev Gastroenterol Hepatol 16: 589-604, 2019.
57. Zhang F, Wei M, Chen H, Ji L, Nie Y and Kang J: The genomic stability regulator PTIP is required for proper chromosome segregation in mitosis. Cell Div 17: 5, 2022.
58. Liu B and Li Z: PTIP-associated protein 1: More than a component of the MLL3/4 complex. Front Genet 13: 889109, 2022.
59. Cheng Q, Xie H, Zhang XY, Wang MY, Bi CL, Wang Q, Wang R and Fang M: An essential role for PTIP in mediating Hox gene regulation along PcG and trxG pathways. FEBS J 289: 6324-6341, 2022.
60. Xu Y, Zhu D, Yang Q, Su D and Chen YQ: PTIP deficiency in B lymphocytes reduces subcutaneous fat deposition in mice. Biochemistry (Mosc) 86: 568-576, 2021.
61. Callen E, Zong D, Wu W, Wong N, Stanlie A, Ishikawa M, Pavani R, Dumitrache LC, Byrum AK, Mendez-Dorantes C, *et al*: 53BP1 Enforces distinct pre- and post-resection blocks on homologous recombination. Mol Cell 77: 26-38.e7, 2020.
62. Das P, Veazey KJ, Van HT, Kaushik S, Lin K, Lu Y, Ishii M, Kikuta J, Ge K, Nussenzweig A and Santos MA: Histone methylation regulator PTIP is required to maintain normal and leukemic bone marrow niches. Proc Natl Acad Sci USA 115: E10137-E10146, 2018.
63. Cenik BK and Shilatifard A: COMPASS and SWI/SNF complexes in development and disease. Nat Rev Genet 22: 38-58, 2021.
64. Wu J, Prindle MJ, Dressler GR and Yu X: PTIP regulates 53BP1 and SMC1 at the DNA damage sites. J Biol Chem 284: 18078-18084, 2009.
65. Chang J, Wu H, Wu J, Liu M, Zhang W, Hu Y, Zhang X, Xu J, Li L, Yu P and Zhu J: Constructing a novel mitochondrial-related gene signature for evaluating the tumor immune microenvironment and predicting survival in stomach adenocarcinoma. J Transl Med 21: 191, 2023.
66. Li P, Yu Z, He L, Zhou D, Xie S, Hou H and Geng X: Knockdown of FOXK1 inhibited the proliferation, migration and invasion in hepatocellular carcinoma cells. Biomed Pharmacother 92: 270-276, 2017.
67. Yang L, Peng F, Qin J, Zhou H and Wang B: Downregulation of microRNA-196a inhibits human liver cancer cell proliferation and invasion by targeting FOXO1. Oncol Rep 38: 2148-2154, 2017.
68. Noh JH, Chang YG, Kim MG, Jung KH, Kim JK, Bae HJ, Eun JW, Shen Q, Kim SJ, Kwon SH, *et al*: MiR-145 functions as a tumor suppressor by directly targeting histone deacetylase 2 in liver cancer. Cancer Lett 335: 455-462, 2013.
69. Wei T, Weiler SME, Tóth M, Sticht C, Lutz T, Thomann S, De La Torre C, Straub B, Merker S, Ruppert T, *et al*: YAP-dependent induction of UHMK1 supports nuclear enrichment of the oncogene MYBL2 and proliferation in liver cancer cells. Oncogene 38: 5541-5550, 2019.
70. Wang L, Zhao Z, Meyer MB, Saha S, Yu M, Guo A, Wisinski KB, Huang W, Cai W, Pike JW, *et al*: CARM1 methylates chromatin remodeling factor BAF155 to enhance tumor progression and metastasis. Cancer Cell 25: 21-36, 2014.
71. Todisco S, Convertini P, Iacobazzi V and Infantino V: TCA cycle rewiring as emerging metabolic signature of hepatocellular carcinoma. Cancers (Basel) 12: 68, 2019.
72. Li F, Wang S, Cui X, Jing J, Yu L, Xue B and Shi H: Adipocyte utx deficiency promotes high-fat diet-induced metabolic dysfunction in mice. Cells 11: 181, 2022.
73. Daniel JA, Santos MA, Wang Z, Zang C, Schwab KR, Jankovic M, Filsuf D, Chen HT, Gazumyan A, Yamane A, *et al*: PTIP promotes chromatin changes critical for immunoglobulin class switch recombination. Science 329: 917-923, 2010.
74. Callen E, Faryabi RB, Luckey M, Hao B, Daniel JA, Yang W, Sun HW, Dressler G, Peng W, Chi H, *et al*: The DNA damage- and transcription-associated protein paxip1 controls thymocyte development and emigration. Immunity 37: 971-985, 2012.
75. Miao Y, Li Z, Feng J, Lei X, Shan J, Qian C and Li J: The role of $CD4^{+}$T cells in nonalcoholic steatohepatitis and hepatocellular carcinoma. Int J Mol Sci 25: 6895, 2024.
76. Zheng X, Jin W, Wang S and Ding H: Progression on the roles and mechanisms of tumor-infiltrating T lymphocytes in patients with hepatocellular carcinoma. Front Immunol 12: 729705, 2021.